GJI | gji_4713 | Dispatch: July 10, 2010 | CE: XCE
Journal | MSP No. | No. of pages: 17 | PE: JM

Geophys. J. Int. (2010) doi: 10.1111/j.1365-246X.2010.04713.x

Shallow subsurface structure of the 2009 April 6 M_w 6.3 L'Aquila earthquake surface rupture at Paganica, investigated with ground-penetrating radar

Q1

Gerald P. Roberts,[1] Bansri Raithatha,[1] Giancanio Sileo,[2] Alberto Pizzi,[3] Stefano Pucci,[4] Joanna Faure Walker,[1] Max Wilkinson,[5] Ken McCaffrey,[5] Richard J. Phillips,[6] Alessandro M. Michetti,[2] Luca Guerrieri,[7] Anna Maria Blumetti,[7] Eutizio Vittori,[7] Patience Cowie,[8] Peter Sammonds,[1] Paolo Galli,[9] Paolo Boncio,[3] Charlie Bristow[1] and Richard Walters[10]

[1]*Research School of Earth Sciences, Birkbeck/UCL, University of London, Gower Street,* WC1E 6BT, *UK. E-mail: gerald.roberts@ucl.ac.uk*
[2]*Università degli Studi dell'Insubria–Sede di Como, Facoltà di Scienze MM. FF. NN., Dipartimento di Scienze Chimiche ed Ambientali, Via Valleggio,* 11–22100 *Como, Italy*
[3] *Dipartimento di Scienze della Terra Università 'G. d'Annunzio' Chieti Campus Universitario,* 66013 *Chieti, Italy*
[4]*Istituto Nazionale di Geofisica e Vulcanologia Sismologia e Tettonofisica, Via di Vigna Murata,* 605 00143 *Roma, Italy*
[5]*Department of Earth Sciences, Durham University, Science Labs, Durham* DH1 3LE, *UK*
[6]*Institute of Geophysics and Tectonics, School of Earth and Environment, University of Leeds,* LS2 9LT, *UK*
[7]*Geological Survey of Italy, ISPRA–High Institute for the Environmental Protection and Research, Via Curtatone,* 3–00185 *Roma, Italy*
[8]*Institute of Geography, School of GeoSciences, University of Edinburgh, Drummond Street, Edinburgh* EH8 9XP, *Scotland, UK*
[9]*Dipartimento della Protezione Civile Nazionale, Rome, Italy*
[10]*COMET, Department of Earth Sciences, University of Oxford, Oxford, UK*

Accepted 2010 June 22. Received 2010 June 22; in original form 2010 March 19

SUMMARY

The shallow subsurface structure of the 2009 April 6 M_w 6.3 L'Aquila earthquake surface rupture at Paganica has been investigated with ground penetrating radar to study how the surface rupture relates spatially to previous surface displacements during the Holocene and Pleistocene. The discontinuous surface rupture stepped between en-echelon/parallel faults within the overall fault zone that show clear Holocene/Pleistocene offsets in the top 10 m of the subsurface. Some portions of the fault zone that show clear Holocene offsets were not ruptured in 2009, having been bypassed as the rupture stepped across a relay zone onto a fault across strike. The slip vectors, defined by opening directions across surface cracks, indicate dip-slip normal movement, whose azimuth remained constant between 210° and 228° across the zone where the rupture stepped between faults. We interpret maximum vertical offsets of the base of the Holocene summed across strike to be 4.5 m, which if averaged over 15 kyr, gives a maximum throw-rate of 0.23–0.30 mm yr^{-1}, consistent with throw-rates implied by vertical offsets of a layer whose age we assume to be ~33 ka. This compares with published values of 0.4 mm yr^{-1} for a minimum slip rate implied by offsets of Middle Pleistocene tephras, and 0.24 mm yr^{-1} since 24.8 kyr from palaeoseismology. The Paganica Fault, although clearly an important active structure, is not slipping fast enough to accommodate all of the 3–5 mm yr^{-1} of extension across this sector of the Apennines; other neighbouring range-bounding active normal faults also have a role to play in the seismic hazard.

Key words:

Q2

GJI Seismology

1 INTRODUCTION

The 2009 April 6 M_w 6.3 L'Aquila earthquake ruptured a fault zone running through the town of Paganica, evidenced by field observations of surface ruptures (Emergeo Working Group 2009; Falcucci *et al.* 2009; Galli *et al.* 2009; ISPRA Report 2009; Messina *et al.* 2009; Boncio *et al.* 2010; Wilkinson *et al.* 2010), and fringe geometries defined by InSAR (Atzori *et al.* 2009; Walters *et al.* 2009; Papanikolaou *et al.* 2010) (Fig. 1). The surface ruptures exhibited maximum surface throws of 7–12 cm, which are consistent with global values expected for earthquakes of this magnitude (Fig. 2; Wells & Coppersmith 1994). The fault had been

Q3

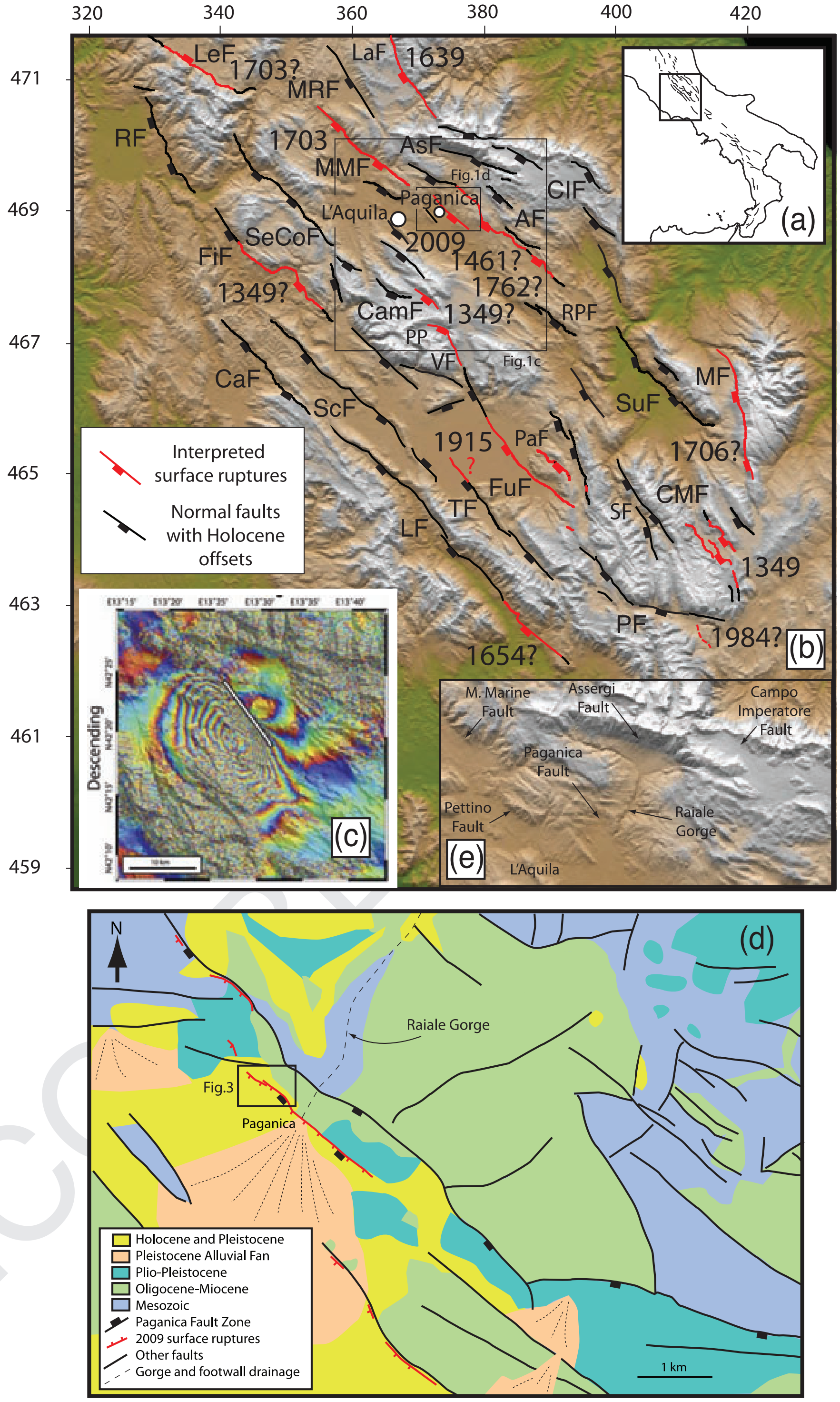

Figure 1. (a) and (b) Map of active faults with Holocene offsets in central Italy, with interpreted positions of historical surface ruptures. Holocene offsets are commonly indicated by the presence of bedrock fault scarps that occur along most of the faults shown (see Table 1). Rupture traces are adapted from our own interpretation of shaking intensities documented in http://storing.ingv.it/cfti4med/, with guidance from Pantosti *et al.* (1996); Pace *et al.* (2002); Basili *et al.* (2008) ; Galli *et al.* (2008) and a large number of papers cited therein. Note that the positions of many of the historical surface ruptures are equivocal and are discussed in this paper. (c) InSAR fringes (28 mm) and modelled fault trace to the 2009 April 6 M_w 6.3 L'Aquila earthquake from Walters *et al.* (2009) and (d) Geological map around the town of Paganica, located in (b), modified from Vezzani & Ghisetti (1987); APAT 2005. Surface ruptures are schematic, but are shown in more detail in Emergeo 2009, Falcucci *et al.* 2009, ISPRA Report 2009 and Boncio *et al.* 2010. (e) Detail of a 20 m DEM, showing the dramatic geomorphic expressions of range-bounding normal faults, and the subdued geomorphic expression of the Paganica Fault. Rf = Rieti Fault; LeF = Leonessa Fault; MRF = Montereale Fault; LF = Laga Fault; MMF = Mt Marine Fault; AsF = Assergi Fault; CIF = Campo Imperatore Fault; AF = L'Aquila Fault; SeCoF = Sella di Corno Fault; FiF = Fiamignano Fault; CamF = Campo Felice Fault; CaF = Carsoli Fault; PP = Piano di Pezza fault; VF = Velino Fault; ScF = Scurcola Fault; FuF = Fucino Fault; TF = Trassaco Fault; LF = Liri Fault; SuF = Sulmona Fault; MF = Maiella Fault; CMF = Cinque Miglia Fault; SF = Scanno Fault; PF = Pescasseroli Fault; CaSF = Cassino South Fault; Parasano Fault; Roccapreturo Fault.

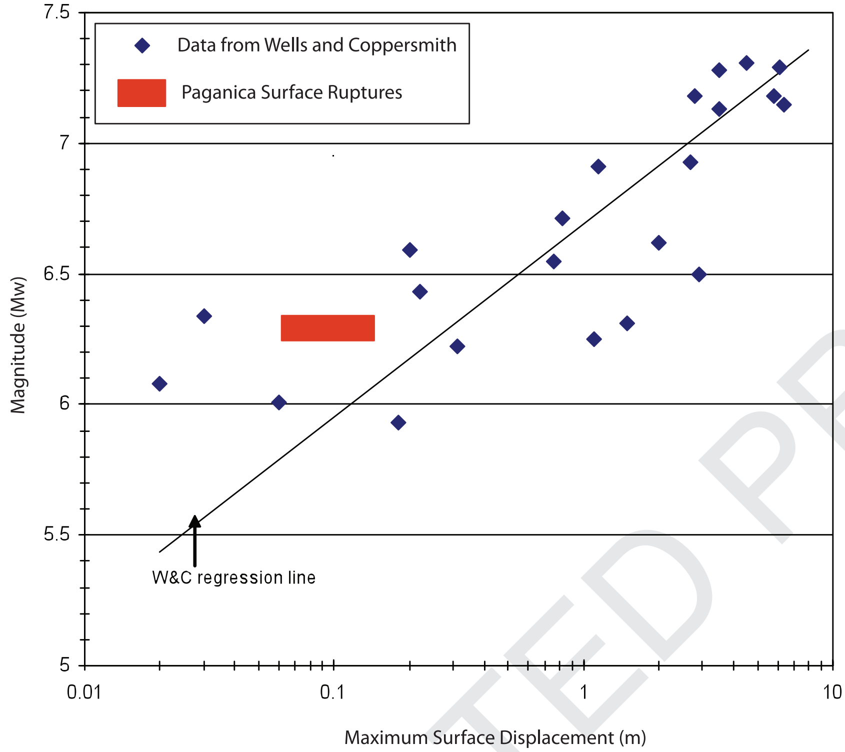

Figure 2. Coseismic throw for the 2009 April 6 M_w 6.3 L'Aquila earthquake plotted alongside data for other normal faulting earthquakes from Wells & Coppersmith (1994).

recognized prior to the earthquake, but its slip rate was poorly defined (see Carta Geologica d'Italia Teramo 1962; Bagnaia *et al.* 1992; Vezzani & Ghisetti 1998; Boncio *et al.* 2004; APAT 2005; Pace *et al.* 2006). The slip-rate was poorly defined because (1) the ruptured fault displays a subdued geomorphic expression, lacking an exposed fault plane along an extensive bedrock scarp, at least near the centre of the ruptures at Paganica, that typifies other active faults in the area (Galadini & Galli 2000; Roberts & Michetti 2004; Papanikolaou *et al.* 2005) (see Table 1) and (2) to our knowledge, no detailed palaeoseismic studies of this fault zone had been published prior to the earthquake. Thus, it was unclear how the Paganica fault zone related, in terms of its slip-rate, to neighbouring range-bounding faults that have more obvious geomorphic signs of Holocene activity such as bedrock scarps, and have published values for their slip-rate defined by palaeoseismic studies (Fig. 1; Table 1).

The observations in this paper address the uncertainty regarding Holocene slip-rates, the rate of deformation and implied earthquake recurrence intervals associated with the Paganica fault zone. We show that the portion of the fault zone within which the 2009 ruptures occurred contains faults whose individual Holocene vertical offsets are small (<4.5 m) implying throw-rates averaged since 15 kyrs of 0.23–0.30 mm yr^{-1}. These individual faults are arranged in en-echelon/parallel geometries, so throw-rates should be summed across strike. However, we find no evidence for summed throw-rates high enough to accommodate measured rates of regional extension (3–5 mm yr^{-1}; D'Agostino *et al.* 2008), implying that at least some of the faults mapped by others (see Fig. 1a and Table 1; Bosi 1975; Vittori 1994; Giraudi & Frezzotti 1995; Galadini & Galli 2000; Michetti *et al.* 2000; Galli *et al.* 2002; Pizzi *et al.* 2002; Roberts & Michetti 2004; Papanikolaou *et al.* 2005; Pace *et al.* 2006; Roberts 2008) along range-bounding escarpments are active and contribute to the extension, consistent with published palaeoseismic studies (Galli *et al.* 2008).

2 BACKGROUND TO ACTIVE FAULTS, EARTHQUAKE SURFACE RUPTURES, SLIP-RATES AND FAULT SCARP MORPHOLOGIES NEAR L'AQUILA

The area around L'Aquila is part of the zone containing active normal faults that stretches from the northern Apennines to Calabria (Anderson & Jackson 1987; Michetti *et al.* 2000; Valensise & Pantosti 2001a; Pace *et al.* 2006; Basili *et al.* 2008; Roberts 2008) (Fig. 1). Historical earthquakes, and those recorded by palaeoseismology, have produced coseismic surface ruptures with vertical offsets that are at least as large as 0.1–2.0 m (Uria de Llanos 1703; Oddone 1915; Westaway & Jackson 1987; Pantosti *et al.* 1993; Q7 Blumetti 1995; Pantosti *et al.* 1996; Galli *et al.* 2008; see Palumbo Q8 *et al.* 2004 for possible evidence of even larger amounts of coseismic surface slip). Such coseismic surface offsets, if repeated in large magnitude earthquakes, would produce a clear expression in the geomorphology in the form of prominent scarps along the active faults (Blumetti *et al.* 1993). However, here we point out that the form of the scarp varies, depending on the local lithologies, sedimentation and erosion rates and the rates and cumulative amounts of vertical offset (including the durations of interseismic periods) across the active fault at each site in question. This suggests three main scarp forms, which are described below, although note these

Table 1. Throw-rates on faults around L'Aquila based on offsets across post-glacial fault scarps (12–18 kyrs), palaeoseismological trench investigations and offset landforms and sediments.

Fault name	Observation	Throw-rate (mm yr^{-1})	Reference
Paganica	GPR and trench data	<0.23–0.3	This paper
Paganica	Offset Quaternary terraces with Tephras	>0.4	Messina *et al.* (2009)
Assergi	Quaternary? Holocen offset	0.7–1.0	Barchi *et al.* (2000); Pizzi *et al.* (2002)
Cinque Miglia	Trench into Holocene	0.3–0.5	D'Addezio *et al.* (2001)
Mte. Marine	Post-glacial scarp 15 ± 3 ka	0.7 ± 0.3	Faure Walker (2010)
Mte. Marine	Offset of late Pleistocene slopes and trenches	0.25–0.43	Galadini & Galli (2000)
Campo Felice	Post-glacial scarp 15 ± 3 ka	0.6 ± 0.2	Faure Walker (2010)
Campo Felice	Offset moraines	0.8–1.3	Galadini & Galli (2000)
Campo Imperatore	Post-glacial scarp 15 ± 3 ka	1.7 ± 0.7	Faure Walker (2010)
Campo Imperatore	Post-glacial scarp 18 ka	0.8–1.0	Giraudi & Frezzotti (1995)
Campo Imperatore	Trench into Holocene	>0.68	Galli *et al.* (2002)
Assergi	Post-glacial scarp 15 ± 3 ka	0.9 ± 0.3	Papanikolaou *et al.* (2005)
Fiamignano	Post-glacial scarp 15 ± 3 ka	1.0	Papanikolaou *et al.* (2005)
Fucino	Offsets of late-Pleistocene and Holocene deposits	0.37–0.43	Galadini & Galli (2000)
Fucino (Ovindoli-Pezza)	Offsets of 0.5 Ma tephras	0.5–1.0	Valensise & Pantosti (2001)
Fucino	Trench into Holocene	0.7–1.2	Pantosti *et al.* (1996), D'Addezio *et al.* (1996)
Fucino	Summed rate on the San Benedetto dei Marsi Holocene trench and Parasano and Ventrino post-glacial scarps	2.0	Roberts & Michetti (2004)
Laga	Offsets of late-Pleistocene and Holocene deposits	0.7–0.9	Galadini & Galli (2000)
Mte. Ocre	GPR, trench and scarp data	0.2 ± 0.1	Salvi *et al.* (2003)
Parasano	Post-glacial scarp 15 ± 3 ka	0.6 ± 0.2; 0.7 ± 0.0.3; 0.4 ± 0.2	Faure Walker *et al.* (2009)
Pescasseroli	Post-glacial scarp 15 ± 3 ka	0.6 ± 0.2	Roberts & Michetti (2004)
Pettino	Offset of alluvial terrace	0.47–0.86	Galadini & Galli (2000)
Roccapreturo	Post-glacial scarp 15 ± 3 ka	0.3 ± 0.7	Faure Walker (2010)
Roccapreturo	Offset of 0.15–1.5 Ma landforms	0.33–0.43	Bertini & Bosi (1993), Galadini & Galli (2000)
Trassaco Fault	Post-glacial scarp 15 ± 3 ka	0.5 ± 0.2	Faure Walker (2010)
Tre Monti	Post-glacial scarp 15 ± 3 ka	0.2–0.5	Faure Walker (2010)
Velino-Magnola	Post-glacial scarp 15 ± 3 ka	0.7	Piccardi *et al.* (1999)
Velino-Magnola	Post-glacial scarp 15 ± 3 ka	0.6 ± 0.2	Faure Walker (2010)

Notes: Where a fault has several values, the values do not conflict because values are reported for different positions along the strike of the fault in question, reflecting throw-rate gradients along strike. A more complete review of throw-rates in Lazio Abruzzo is given in Faure Walker (2010). Alternative reviews are given by Galadini & Galli (2000) and Pace *et al.* (2006).

forms are a continuum of scarp morphologies (values given for rates are indicative rather than exact values; refer to Table 1 for examples near L'Aquila).

(1) Type 1 Scarps—with high throw-rates (>0.2–0.4 mm yr^{-1}), low erosion and sedimentation rates (<0.2–0.4 mm yr^{-1}) and cumulative offsets of several hundred metres or more of pre-rift strata (Mesozoic/Tertiary), bedrock scarps form along the active normal faults (if the bedrock is carbonate that is resistant to erosion) (see Piccardi *et al.* 1999; Galadini & Galli 2000; Roberts & Michetti 2004; Papanikolaou *et al.* 2005 or examples, such as those along the Velino, Assergi, Mt Marine, Campo Imperatore, L'Aquila and Sulmona faults shown in Fig. 1b). Such bedrock scarps offset slopes formed during the high erosion and sedimentation rates that existed during the last glacial maximum (*ca.* 18 ka) (see Roberts & Michetti 2004 for details), and hence post-date this age. Such ages have been proved through *in situ* ^{36}Cl cosmogenic exposure dating, with fault planes on the bedrock scarps dated to ~12 ka in the Apennines (e.g. Palumbo *et al.* 2004; Schlagenhauf 2010). Such sites will form where there is a relatively small sediment flux from the footwall of the normal fault, and as such, will be characterized by the lack of local footwall drainage courses.

(2) Type 2 Scarps—where sedimentation rates are higher, such as where active faults cross alluvial fans at the mouths of footwall drainage courses, yet throw-rates are still >0.2–0.4 mm yr^{-1}, the scarp may be subtle, or obscured. In such cases activity on the fault can be proven if a palaeoseismic trench is excavated with a view towards examining offsets of Holocene sediments (see Michetti *et al.* 1996; Pantosti *et al.* 1996; Galli *et al.* 2002; Galli *et al.* 2008 for examples along the Fucino/Piano di Pezza, Campo Imperatore and Cinque Miglia Faults). At such sites, Holocene organic-rich sediment, with human artefacts in places, such as ceramics, overlie organic-poor Pleistocene conglomerates/breccias that formed during and prior to the last glacial maximum. Alternatively, geophysical techniques such as ground-penetrating radar can be used to image offsets of the Holocene (e.g. Salvi *et al.* 2003; Jewell & Bristow 2004).

(3) Type 3 Scarps—if throw-rates on the fault are low (<0.2–0.4 mm yr^{-1}), subtle scarps in Quaternary/Holocene sediment can be preserved if the sedimentation/erosion rates are also <0.2–0.4 mm yr^{-1}. Such low throw-rates typically result in relatively small cumulative vertical offsets (<1 km) in the Apennines because faults have only been active since ~2–3 Ma or less, and relatively small vertical offsets of the Holocene (< ~4–6 m if organic-rich sediments started to form during the demise of the last glacial maximum at 15–18 ka). Such sites will form where there is a very low sediment flux from the footwall of the normal fault (<0.2–0.4 mm yr^{-1} sedimentation

rate), and as such, will be characterized by the lack of obvious footwall drainage courses. Such sites are relatively uncommon in the literature (although see Salvi *et al.* 2003 for a possible example). Offsets of the Holocene are needed to prove activity, and this can be achieved by palaeoseismic trenching or using shallow geophysical techniques. Such subtle scarps can be disturbed and hence obscured by human activity.

Prior to the 2009 L'Aquila earthquake, the ruptured fault near Paganica, downthrowing Holocene and Pleistocene continental deposits against post-Mesozoic sediments, where exposed NW of the large, incised footwall drainage course of the Raiale gorge (Fig. 1d), was considered by some of the present authors to be a possible example of a Type 3 morphology. This is because no clear bedrock scarp was obvious near Paganica (the nearest being on en echelon structures to the NW—see Boncio *et al.* 2010), yet the lack of obvious drainage courses immediately in the footwall of the scarp has allowed preservation of a subtle and perhaps equivocal 4–5-m high scarp in colluvium on a *ca*. 150-m wide, 20–30-m high escarpment (Figs 3c and d). If this equivocal scarp was indeed an indicator of fault activity, and not modified by human activity, the above implies that the throw-rate would be relatively low compared to other faults around L'Aquila (Table 1), perhaps with a throw-rate value of $<$0.2–0.4 mm yr^{-1}, although we emphasize that we are aware of no palaeoseismic study confirming such values published prior to the earthquake. Such low rates of activity on the Paganica fault zone may be supported by the observation that the total vertical offset of Mesozoic-Cenozoic strata across the fault is 200–300 m, a value that is small compared to neighbouring faults that have throws of 600–1200 m (e.g. Mt Marine & Assergi Faults; see Pizzi *et al.* 2002; Roberts & Michetti 2004). If it is assumed that all the faults started to slip at the same time (2–3 Ma or less; see Roberts & Michetti 2004 for a discussion), the observation of relatively small post-Mesozoic throw is consistent with low throw-rates and a Type 3 Scarp at Paganica. Despite the low throw-rates envisaged for the Paganica fault zone, evidence for active faulting was present and recognized, in the form of incised footwall drainage. The Raiale gorge (Figs 1d and e), incises down into the footwall of the Paganica fault zone, with incision ending at the fault trace, indicating differential vertical motions across the fault in the Quaternary. We are aware of no studies published prior to the earthquake that used observations of incision to derive a throw-rate for the Paganica fault zone. Since the earthquake, Messina *et al.* (2009) have examined tephras around the Paganica fault zone to study rates of vertical offset. Through microprobe and lithological comparison of fresh glass shards with dated tephras from elsewhere in Italy, they identify tephras that may correlate with eruptions of the Colli Albani and Sabatini volcanoes in western Italy at ∼560, ∼456, ∼450 and ∼360 ka. Messina *et al.* (2009) use these ages alongside the elevations of the tephras to suggest a few hundred metres of offset across the Paganica fault zone since the Middle Pleistocene, stating a 'minimum slip-rate of ∼0.4 mm yr^{-1}'. Also, a palaeoseismic study of faults in a trench across the ruptures published since the earthquake (Boncio *et al.* 2010), suggests a throw-rate of 0.24 mm yr^{-1} for post-24.8 kyr activity based on radiocarbon dates.

Other studies discuss the possibility of higher rates of activity on the Paganica fault zone. Pace *et al.* (2006) suggested a possible slip-rate of 0.6 mm yr^{-1} for what they term the 'Paganica Fault'. However, Pace *et al.* (2006) did not provide new data on the rates of deformation, instead citing reviews of regional active fault locations as the source of the value (Barchi *et al.* 2000; Valensise & Pantosti 2001b). Chiarabba *et al.* (2009) suggest that, 'The present observation that the Paganica fault is accommodating the extension in the central Apennines area [3–5 mm yr^{-1} according to D'Agostino *et al.* (2008)] poses unambiguous evidence that at least some of the mapped faults are no longer active' (presumably referring to faults shown in Fig. 1b). Chiarabba *et al.* (2009) also point out that 'the role of the large normal faults, mainly mapped by geomorphologic approach, still needs to be understood' (see Figs 1b and e for maps of such 'large normal faults'); 'Are they representing potential structure for $M > 6.5$ earthquakes, or do they include fossil or creeping segments?' Also, following this theme, that emphasizes the possibility of high rates of activity across the Paganica fault, Tertulliani *et al.* (2009) suggest that the Paganica fault may have been the source of previous $>M6$ historical earthquakes that have caused damage to L'Aquila in 1461 A.D. and 1762 A.D.. However, these authors note that '∼three-centuries recurrence time of the events would be too-short rate when compared to mean recurrence times calculated for other seismogenic faults in peninsular Italy (Galli *et al.* 2008)'.

The above shows that there is some debate regarding the rate of activity on the Paganica fault zone and surrounding faults, and this has implications for the seismic hazard represented by the structures. If the rate of throw accumulation is low compared to other faults in the area, the probability of surface rupture on the Paganica Fault will be low in a given time period compared to that for faults with Type 1 or Type 2 scarp morphologies which are common in this part of the Apennines (see Roberts *et al.* 2004 and Table 1), assuming similar-sized slip events for all these faults. The 2009 L'Aquila earthquake would then be an example of rupture on a fault that had a relatively low probability of rupture. However, the high activity rates suggested by the work of Tertulliani *et al.* (2009) and Chiarraba *et al.* (2009), and the relatively high slip-rate and probability of rupture suggested by Pace *et al.* (2006), mean that the low slip-rate scenario for the Paganica fault suggested above should be re-examined. We have investigated the rates of Holocene activity around the ruptured fault in the Paganica fault zone using ground-penetrating radar to augment observations from a trench produced by water-escape from a pipe ruptured by the L'Aquila earthquake main shock (Falcucci *et al.* 2009; Boncio *et al.* 2010).

3 GEOLOGICAL SETTING OF SURFACE RUPTURES ALONG THE PAGANICA FAULT ZONE

The Paganica fault zone is not composed of a single fault trace; here we describe the architecture of the fault zone in detail. A *ca*. 20 km-long Paganica fault zone is clearly shown on published geological maps of the area (Fig. 1d; Vezzani & Ghisetti 1998; APAT 2005). Where exposed in the Raiale gorge near Paganica, the fault separates a hangingwall succession of Upper Eocene-Miocene marly limestones and calc-arenites overlain by Holocene-Pleistocene fluvioglacial, alluvial, colluvial and lacustrine sediments, from footwall Miocene carbonates and calc-arenites overlying Mesozoic bioclastic carbonates (Fig. 1d). The hangingwall Holocene-Pleistocene sediments are suggested to be a few hundred metres thick (Messina *et al.* 2009), implying that the total throw of the Mesozoic across the Paganica Fault is 200–300 m; however, note that the value may be less as drill holes for water research penetrated limestones (Miocene?) at 30–70 m depth. Importantly, the surface ruptures occurred about 300 m into the hangingwall of the fault offsetting the Mesozoic marked on the map of Vezzani & Ghisetti (1998) Q11

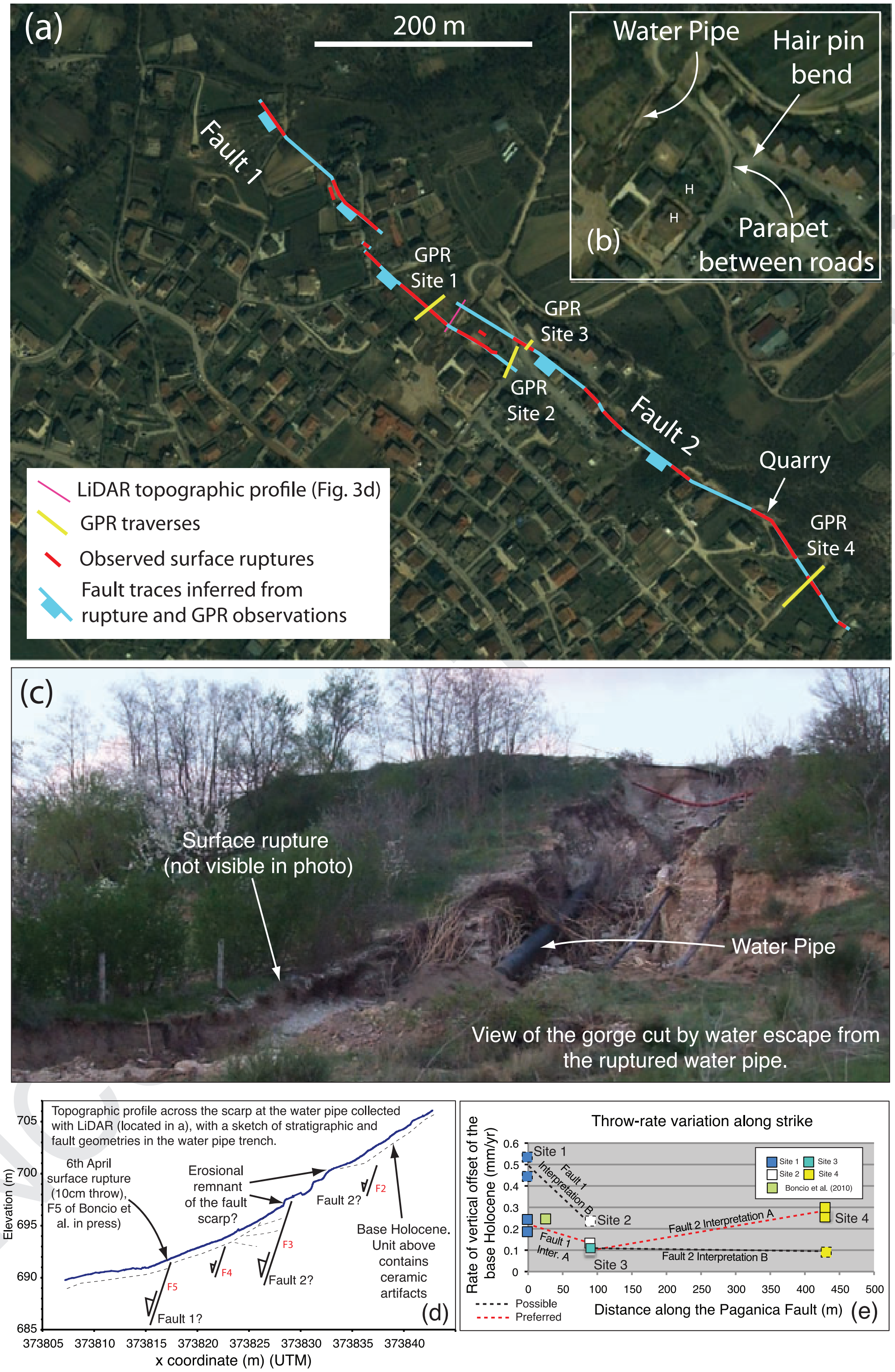

Figure 3. (a) Map of surface ruptures/cracks and subsurface faults inferred from ground-penetrating radar data, overlain on an Ikonos image (located in Fig. 1d). Surface ruptures are schematic as individual cracks spaced a few metres apart across strike cannot be shown at this scale. (b) Inset map showing the location of the water pipe and roads. H = Houses that may be responsible or refraction hyperbolae on Fig. 6. (c) View of the gorge excavated by water escape from the ruptured water pipe. (d) Topographic profile from LiDAR data showing the subtle morphology of the scarp [located in (a)]. Fault 1 and Fault 2 correlate with the same in (a). F2, F3, F4 and F5 in red correlate with fault numbers in Boncio *et al.* (in press). (e) Along-strike-profiles of the rate of vertical Holocene offset (throw-rate) measured with ground-penetrating radar data (summarizing Figs 5, 6, 7 and 8). Uncertainty in throw-rate interpretation is indicated. Note that if the rates from Sites 2 and 3 are summed across strike, a value of 0.2–0.3 mm yr^{-1} is gained; thus the throw-rate profile remains at a constant rate across the relay zone, showing that the faults are sharing the deformation over a Holocene timescale. A tentative correlation between the faults visible in the water-pipe gorge and those interpreted from GPR is shown (compare d and e).

(Fig. 1d). At this location, a fault downthrows Holocene-Pleistocene fluvio-glacial, alluvial, colluvial and lacustrine sediments against an Upper Pleistocene alluvial sequence of sand, silt and conglomerate overlying Oligocene-Miocene carbonates and calc-arenites. It is here that the fault may be expressed as a subtle and perhaps equivocal 4–5-m high scarp on a *ca*. 150-m wide, 20—30-m high escarpment, although the 4–5-m high scarp may be modified by human activity. It appears that most of the post-Middle Pleistocene activity has occurred in this portion of the fault zone (Messina *et al.* 2009). However, it may be that the fault that ruptured in 2009 and the fault offsetting the Mesozoic in the Raiale gorge merge at depth, so we refer to both structures as being part of the Paganica fault zone.

Surface ruptures produced by the 2009 earthquake in the vicinity of the town of Paganica are best displayed NW and SE of the Raiale gorge on an abandoned Pleistocene alluvial fan surface that has been incised by the modern river. The ruptures are a set of discontinuous ground cracks and surface faults that, individually, can be traced for distances of 15–20 m. Together, these discontinuous features form a NW–SE trending zone of surface rupture that, as a semi-continuous structure, can be traced for ∼2.5 km along strike, and are considered to be the un-ambiguous primary surface expression of the earthquake rupture due to its consistency and continuity (Emergeo Working Group 2009; Falcucci *et al.* 2009; ISPRA Report 2009). However, note that other, less continuous ground cracks and ruptures have been reported along a zone that may be as long as 13–19 km in length (see Galli *et al.* 2009; Boncio *et al.* 2010). Vertical offsets of up to 12 cm were measured, as were horizontal opening values across cracks of a similar amount (Boncio *et al.* 2010).

We have chosen to study sites around a water pipe that was ruptured in the earthquake (Fig. 3). The ∼70 cm diameter pipe was at ∼40 bars water pressure, carrying water to the city of L'Aquila from the nearby mountains. The water pipe ruptured in the main shock, as reported by local people, who heard water escaping from the pipe during the early morning of April 6. The ensuing water jet excavated a gorge through Holocene and Pleistocene gravels, allowing examination of the subsurface stratigraphy (Fig. 3c). In the vicinity of the water pipe, the ruptures occurred along a subtle fault escarpment, with the ground rising by 20–30 m over distance of about 150 m (Figs 3c and d). The ruptures occurred about 15 m into the hangingwall of a poorly defined 4–5 m scarp that exists about halfway up the 20–30-m high escarpment (Fig. 3d). In the vicinity of the area we study near the ruptured water pipe, there are no significant footwall drainage courses, and the fan surface has abandoned due to incision of the modern river, so we expected the site to have a very low Holocene sedimentation rate (see below). It is important to note that the scarp and escarpment are not easy to recognize in the field, as the area contains many concrete constructed houses, tarmac/concrete roads and small quarries (Fig. 3a), and has therefore been modified by human activity; the topographic profile we scanned with LiDAR (Fig. 3d), is probably the only relatively un-disturbed portion of the scarp for hundreds of metres along strike, and itself does not cover the entire across-strike width of the escarpment due to building and road construction.

4 METHODS

We scanned the topography using a Riegl 420 terrestrial laser scanner (LiDAR) to make topographic profiles for ground-penetrating radar, supplementing these data with a total station. We used the PulseEkko 100 GPR system, with 200 MHz antennae at five sites along the rupture, of which we report four here, to concentrate on the area shown in Fig. 3. The 200 MHz antennae were spaced 50 cm apart and were repositioned every 10 cm on stepwise-transects. We used Ekko_View Deluxe 42 and EKKO_View software to process the raw data and produce depth converted GPR images of the subsurface. We used a value of 0.1m ns^{-1} to depth convert the data, as this is a typical value for sediment, and we conducted a common midpoint survey (CMP) and a study of short wavelength reflection hyperbolae to constrain this value. We used the following steps and filters to process the data: Q12

(1) Data sets were saved in different files, so the data were merged.
(2) The 'chop time' data option was used to remove the air wave (first layer).
(3) The data were shifted using a velocity of 0.1 m ns^{-1}.
(4) We applied a 'dewow' filter.
(5) The time window was reduced to remove noise from depth.
(6) A vertical time filter was applied to remove high frequency noise.
(7) A spatial median filter (width: 7, Mean: 3): was applied to eliminate noise.
(8) We applied either an Automatic Gain Control (AGC) or a Spreading and Exponential Compensation Gain (SEC) to enhance the quality of the GPR image (Window width: 0.15, Max. value: 800).
(9) We added topography using a.top file of the elevations and distances obtained from the LiDAR and/or total station.

We also mapped the ruptures in the field within a few hundred metres of the ruptured water pipe using hand-held GPS receivers (see Emergeo Working Group 2009; Galli *et al.* 2009, ISPRA Report 2009; Boncio *et al.* 2010 for more extensive mapping), and measured the kinematics of the ruptures using a compass and clinometer.

5 RESULTS

First, we augment the observations of Emergeo Working Group (2009); Falcucci *et al.* (2009); Galli *et al.* (2009); ISPRA Report (2009) and Boncio *et al.* (2010) with slip-vector azimuths measured with a compass and clinometer (Fig. 4). Slip-vector azimuths were in the range of 210–232° over a distance of *ca*. 2.5 km along the strike of the fault, with a mean vector azimuth of 218°. The slip-vector azimuth is almost perpendicular to the strike of the ruptures (∼127°), indicating a pre-dominant dip-slip normal motion. This slip-vector azimuth was maintained despite the fact that the rupture was discontinuous and appeared at different heights on the subtle escarpment along the Paganica fault zone. For example, in the area 100 m to the east of the ruptured water pipe, the rupture deviated from its general NW–SE orientation, to run as discontinuous cracks in an E–W direction, climbing in elevation by *ca*. 20–30 m between the water pipe and a hairpin bend on a tarmac road (Figs 3a and b). This elevation was maintained as the discontinuous cracks continued to the SE near and/or through some houses and into a small quarry, before they turned into a NNW–SSE orientation, descending by *ca*. 30 m as the cracks crossed a concrete road (Fig. 3a, Site 4), and then the main tarmac road in the Raiale gorge (Fig. 1d). This change in elevation and strike of the zone containing the discontinuous surface ruptures suggested that the subtle escarpment along the ruptured portion of the fault zone was formed as a result

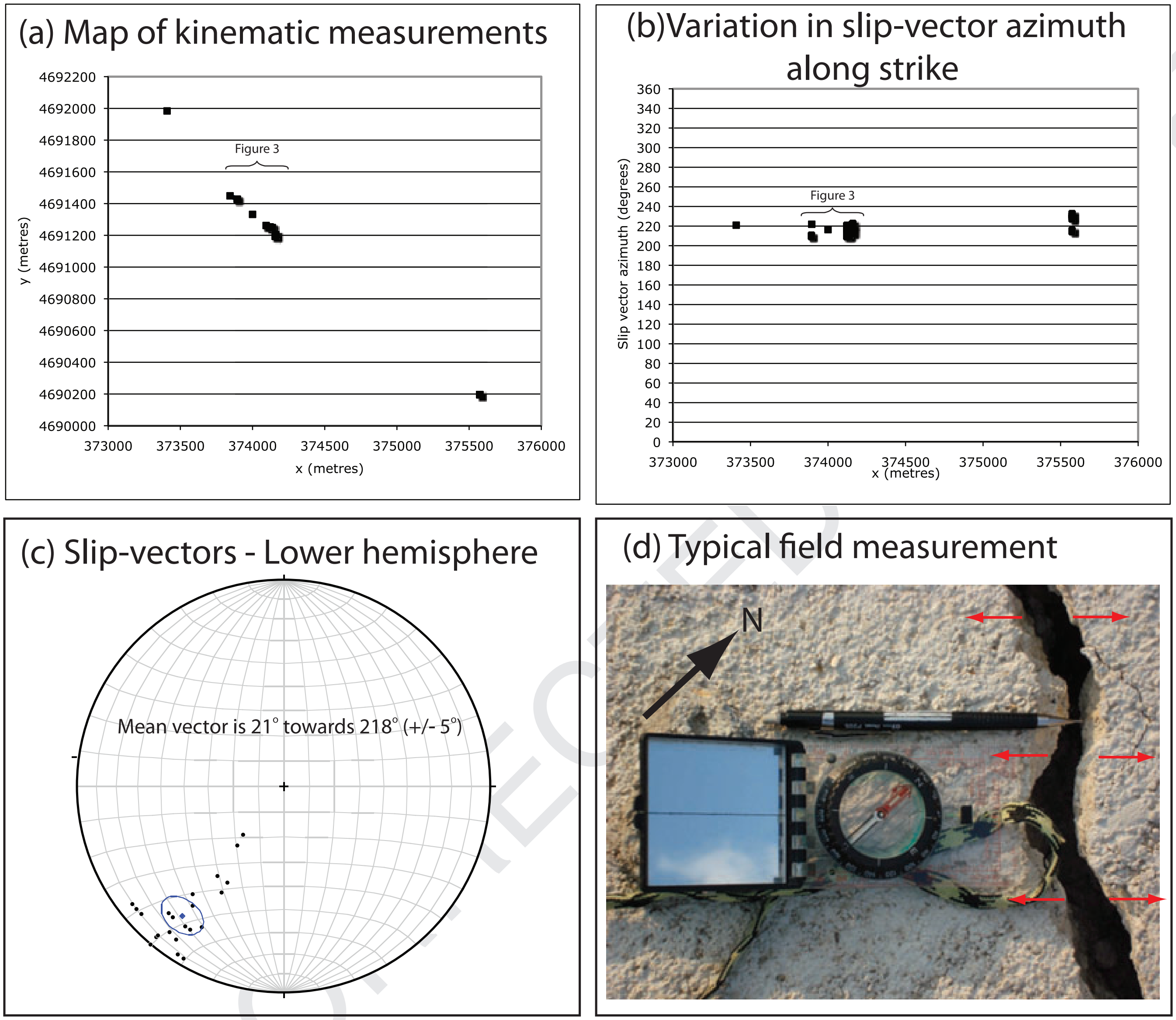

Figure 4. (a) Map of sites from which the kinematics of the 2009 surface ruptures were measured (UTM coordinates). (b) Variation in the slip-vector azimuth along strike measured across ground cracks. Error is similar in size to the symbols. (c) Lower hemisphere stereographic projection of opening vectors across ground cracks from the 2009 ruptures. (d) Typical field measurements supporting (a), (b) and (c) (from the concrete road at Site 4).

of activity on an anastomizing set of small faults that make up the overall fault zone. This is consistent with observations of the fault zone in the trench excavated by water escape from the ruptured water pipe, where at least four faults can be seen at outcrop within the conglomerates, sandstones and soils (Boncio *et al.* 2010; Fig. 3d). It is also consistent with relay zone, en-echelon geometries for the mapped surface ruptures reported along strike, south east of the Raiale gorge (Emergeo Working Group 2009; ISPRA Report 2009, see their Annex 3, (Boncio *et al.* 2010). This prompted the second part of our study to investigate the shallow subsurface structure using ground-penetrating radar to ascertain how the 2009 ruptures relate spatially to previous Holocene and Pleistocene slip within the Paganica fault zone, and possible relay zone structures in the subsurface that do not have a prominent geomorphic expression. Ground-penetrating radar revealed a clear fault zones at four sites (Fig. 3).

5.1 Site 1–20–30 m NW of the ruptured water pipe across a field

In this location, ruptures from the April 6 earthquake were found as three parallel discontinuous fractures spaced 2–3 m apart, associated with bending of the ground surface (Boncio *et al.* 2010). Three palaeoseismological studies of the trench exposed through rupture of the water pipe published since the earthquake have provided radiometric ages for sediments deformed by faults exposed in the trench (Falcucci *et al.* 2009; Galli *et al.* 2009; Boncio *et al.* 2010). Fig. 3d summarizes their findings, showing that a number of faults contribute to the deformation. Boncio *et al.* (2010) suggest a throw-rate of 0.24 mm yr^{-1} for post-24.8 kyr activity measured in the water pipe trench, that is shared between the faults that they name F5, F4 and F3 (see Fig. 3d). The three parallel fractures exposed on the ground surface 20–30 m to the NW appear to correlate with F5 and faults in its footwall (Boncio *et al.* 2010). Below, we attempt to correlate faults and rates of deformation between the water pipe trench and our GPR line 20–30 m to the NW.

A 46-m long GPR survey running NE–SW across the ruptures achieved depth penetration of about 10 m on a topographic slope that decreased in elevation by 20 m over a horizontal distance of 46 m (Fig. 5).

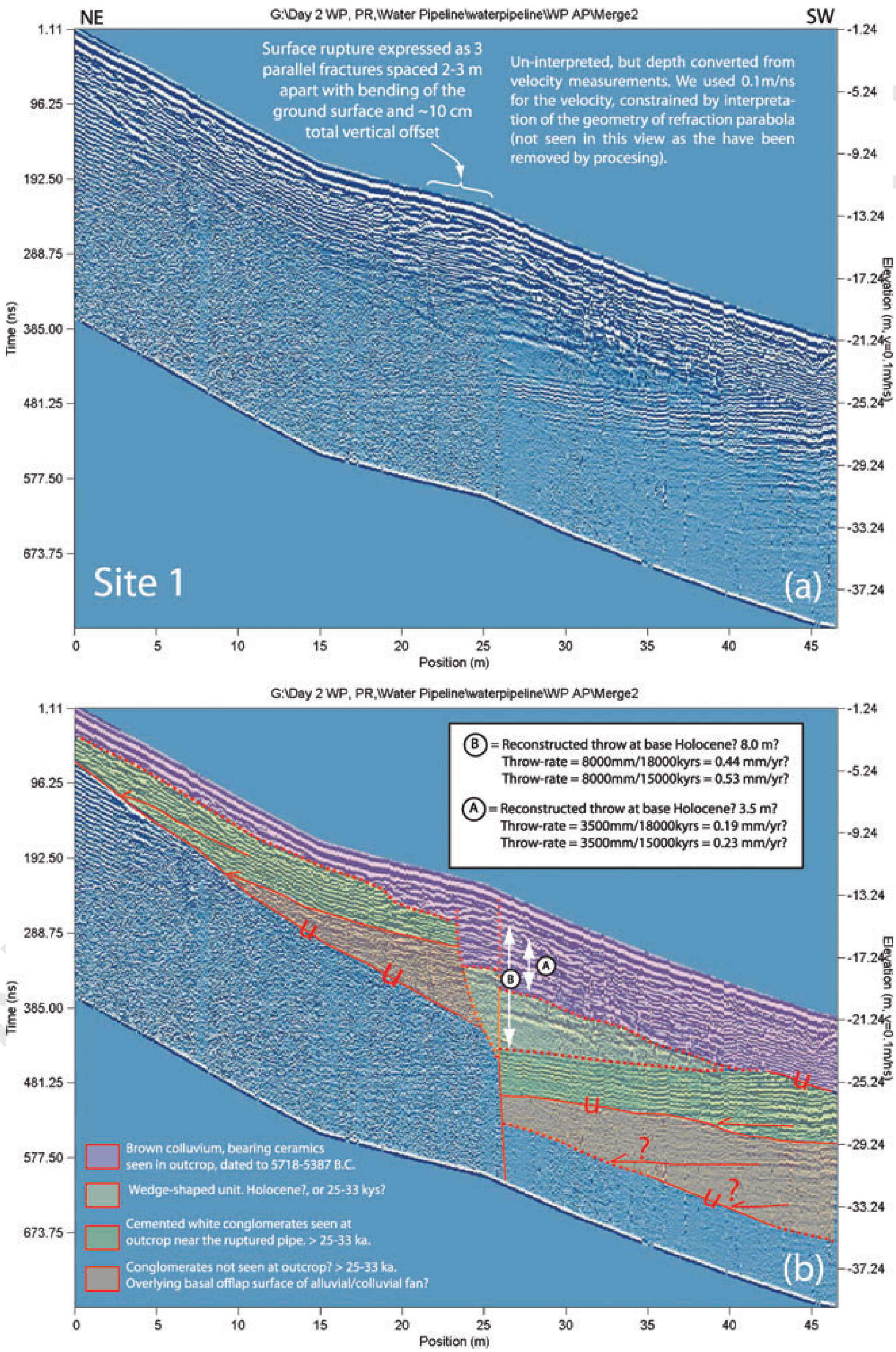

Figure 5. Site 1 (a) Un-interpreted, and (b) interpreted depth converted ground-penetrating radar profiles. Vertical scales are time in nanoseconds and depth in metres. The GPR data were collected on a soil covered slope.

A stratigraphy of cemented, white conglomerates lying beneath ceramic-bearing Holocene colluvium that is exposed in the trench excavated by water escape from the ruptured water pipe (Fig. 3c), has also been imaged in the subsurface using GPR. The cemented, white conglomerates (probably Unit U9 of Boncio *et al.* 2010), are characterized by thin, continuous and parallel radar returns in both the footwall and hangingwall of the rupture. At depth, these returns are offset by a steeply dipping fault(s) on the GPR profile; the vertical offset of this unit is 8 m. As the 2009 earthquake produced only ∼10 cm of vertical motion at this site, the rest of the 8 m offset must be attributed to previous surface faulting along this active fault. Overlying the cemented, white conglomerates both at outcrop and imaged by the GPR, are organic-rich colluvial conglomerates and soil that in places contain ceramic fragments (Boncio *et al.* 2010). These organic-rich colluvial deposits have been dated to 5718 B.C./5467 B.C. to 5403 B.C/5387 B.C. via radiocarbon dating (Falcucci *et al.* 2009), ∼5 kyrs by Boncio *et al.* (2010) and Q13 2.5 ka–900 A.D. with AMS (Galli *et al.* 2009). These Holocene ages are consistent with the organic-rich nature of the sediments and the fact that they contain fragments of ceramics, which must be associated with the youngest reported ages. The base of this Holocene unit is clear in the footwall of the rupture on the GPR profile. The basal contact dips towards the rupture, and incises down into the underlying cemented, white conglomerate in the 4 m closest to the interpreted fault. The base of the Holocene is less easy to interpret in the hangingwall of the fault on the GPR profile. The base Holocene is either (1) a subhorizontal radar return defining the top of the aforementioned white, cemented conglomerate (Interpretation B in Fig. 5b), or (2) is a SW-dipping radar return that is above, and separated from the white, cemented conglomerate by a wedge-shaped unit, truncating the white-cemented conglomerate between 40–46 m along the profile at an angular unconformity (Interpretation A in Fig. 5b). If the former is correct, the vertical offset of the base Holocene across the fault is 8 m implying a throw-rate of 0.53 mm yr^{-1}, assuming an age for this contact of 15 ka (the oldest probable age of organic-rich sediments that would have formed after the demise of the last glacial maximum) (Interpretation B on Fig. 5b). If the latter is correct, the vertical offset of the base Holocene across the fault is a maximum of 3.5 m implying a maximum throw-rate of 0.23 mm yr^{-1}, again assuming an age for this contact of 15 ka (Interpretation A on Fig. 5b). We are unsure which of these two interpretations is correct as we have no age control along the line of the GPR profile. However, combined ^{14}C dating of organic material (34 970 ± 470 BP) and U/Th dating of a tufa fragment (33 000 ± 4100 yr BP) by Falcucci *et al.* (2009) in the neighbouring trench suggests that the wedge-shaped unit may date from ∼33 ka (this probably correlates with units U7 and U8 of Boncio *et al.* 2010, that they dated to 24 890 ± 140 yr BP), supporting our Interpretation A. Thus, we prefer Interpretation A on Fig. 5b, where the rate of Holocene vertical offset is 0.19–0.23 mm yr^{-1}, depending on the age assigned to the base of the ceramic-bearing, organic-rich sediments (15–18 ka). Importantly, this rate is similar to that implied from the offset of the top of the cemented white conglomerate (8 m offset; 33 ka; 0.24 mm yr^{-1}), assuming its age is 33 ka. Also, note that the fault that is clear at depth, truncating the radar returns that we interpret as the white, cemented conglomerate, is not very clear in the Holocene deposits in the GPR data, although field observations confirm that three parallel fractures and a warp of the ground surface formed at precisely this location in the 2009 earthquake. The white, cemented conglomerate underlies the Holocene, and the wedge-shaped unit that probably dates from ∼25–33 ka, and is thus in interpreted to be >25–33 ka, perhaps dating from the Middle or Upper Pleistocene. The white, cemented conglomerate, and an underlying unit that is not exposed at outcrop with less clear radar returns, show possible, but equivocal 'lap' relationships with underlying angular unconformities near the base of imaged section. We tentatively interpret these as offlap of alluvial fan sediments above basal erosional truncation surfaces. However, the base of this unit is poorly imaged and we indicate this with a dashed line and question marks on Fig. 5.

Overall, the fault imaged with GPR has not been directly traced into the water pipe trench due to lack of outcrop, but we suggest an interpretation where it correlates with the surface rupture location shown in Figs 3c and d. Our preferred throw-rate of 0.19–0.23 mm yr^{-1} compares with the rate of 0.24 mm yr^{-1} for post-24.8 kyr activity measured in the water pipe trench, that Boncio *et al.* (2010) suggest is shared between the faults that they name F5, F4 and F3 (see Fig. 3d). We suggest the Holocene throw associated with the fault interpreted on our GPR line may be shared along-strike between faults F5, F4 and F3 of Boncio *et al.* (2010). This may explain why displacements are less on the ruptured fault F5 in the water pipe trench (1.0 m, Boncio *et al.* 2010) compared to the ruptured fault imaged with GPR (3.5 m). Note that in this interpretation, the location of the ruptured fault does not coincide exactly with the poorly defined scarp measured with LiDAR (Fig. 3d). Instead, the rupture is ∼20 m into the hangingwall, with Holocene slip shared possibly between faults F5, F4 and F3. The degraded nature of the scarp suggests that it may be an erosional feature on the unconsolidated slope, where a fault scarp associated with three closely spaced subsurface faults (F5, F4 and F3) has formed, eroded and thus retreated upslope, and not a simple fault scarp. Thus, although more strain may be accommodated across strike of the ruptured fault, we have found no evidence for rates of Holocene throw accumulation higher than 0.23–0.30 mm yr^{-1}.

5.2 Sites 2 and 3–70 m SE of the ruptured water pipe across tarmac roads

Site 2 is a 38-m long survey running NE–SW along a tarmac road that achieved depth penetration of about 10 m on a topographic slope that decreased in elevation by 10 m over a horizontal distance of 38 m (Fig. 6). This survey did not cross the rupture (Fig. 3), but was along strike from Site 1, and across strike from Site 3. Site 3 is a 16-m long survey running NE–SW across a hairpin bend in a tarmac road (Fig. 7). It achieved depth penetration of about 10 m on a topographic slope that decreased in elevation by 2 m over a horizontal distance of 16 m. This survey did cross the rupture, which offset the surface of the tarmac road. Although Sites 2 and 3 appear quasi-continuous on the map in Fig. 3, they are separated by a vertical drop of several metres across a concrete road parapet (Fig. 3b), explaining why we did not combine these sites into a single survey. Site 3 is also *ca*. 8 m along strike from Site 2. However, as they neighbour each other, we interpret them together.

Sites 2 and 3 appear to show very similar stratigraphic patterns to that at Site 1. We use the stratigraphy in the trench at the ruptured water pipe (70 m away to the NW), and comparison of radar-return patterns from Site 1 to aid our interpretation. Our interpretation of Site 2 is complicated by the existence of possible hyperbolic reflections produced by air returns from a nearby concrete house. The radar signal is non-directional, and hence can sample objects above the ground surface, erroneously placing them at depth; such air-return signals can be recognized because they have relatively long wavelength, hyperbolic shapes. Site 2 runs close to

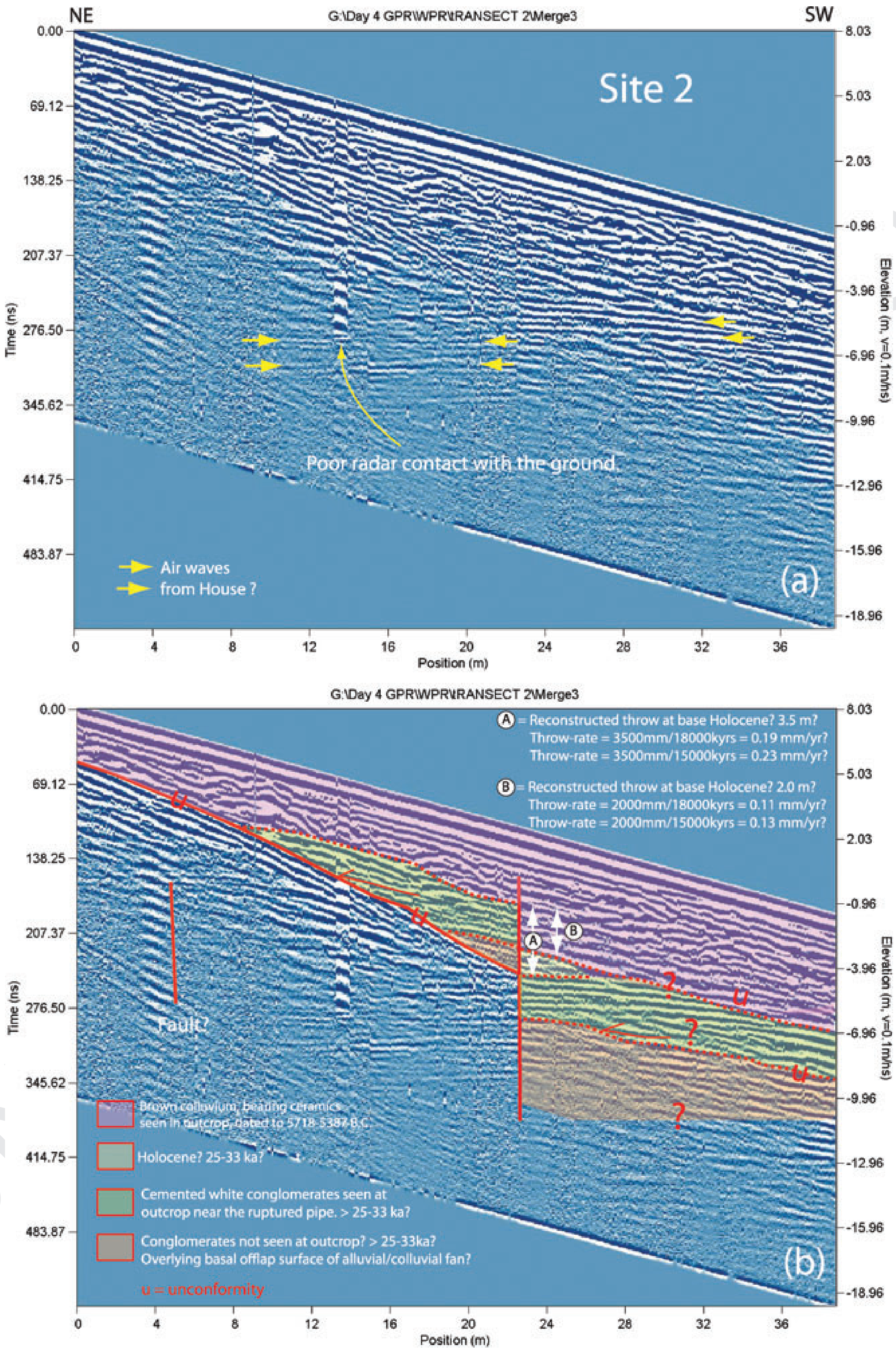

Figure 6. Site 2 (a) Un-interpreted, and (b) interpreted depth converted ground-penetrating radar profiles. Vertical scales are time in nanoseconds and depth in metres. The profile was collected on a tarmac road. Convex upwards hyperbolae in the upper part of the section are interpreted to be from point sources (subsurface boulders?). Long wavelength hyperbolae in the lower right of the view may be air returns from nearby houses (see Fig. 3), producing uncertainty in the interpretation of the hangingwall geometry indicated with 'question marks'.

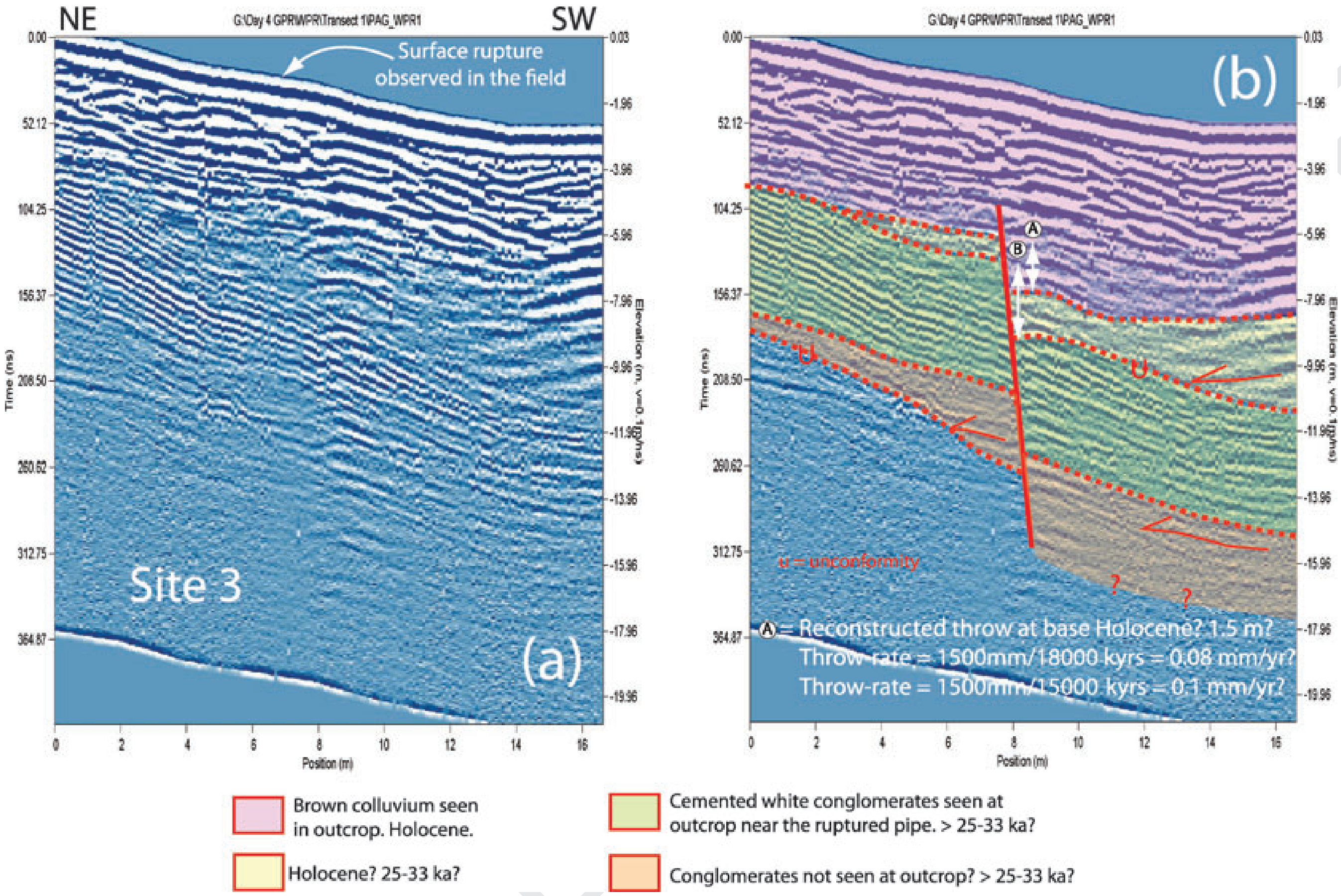

Figure 7. Site 3 (a) Un-interpreted, and (b) interpreted depth converted ground-penetrating radar profiles. Vertical scales are time in nanoseconds and depth in metres. The profile was collected on a tarmac road.

a concrete house, and we note the existence of possible examples of hyperbolic reflections from this house in the data from Site 2 (Fig. 6a).

Despite the occurrence of possible hyperbolic reflections produced by air returns from a nearby house, we suggest that Site 2 shows truncation of radar returns at depth that resemble a fault. In detail, we interpret thin, continuous and parallel radar returns in the hangingwall as the lateral continuation of the white, cemented (>25–33 ka) conglomerates that crop out in the water pipe trench. The white, cemented conglomerate is therefore downfaulted at this site. These thin, continuous and parallel radar returns are separated from overlying sediment by a possible angular unconformity, similar to that noted at Site 1. This angular unconformity also exists in the footwall, allowing us to reconstruct the vertical offset. We interpret the material above the angular unconformity to be the ceramic-bearing, organic-rich colluvial conglomerates, sandstones and soil that have been dated to 5718 BC/5467 BC to 5403 BC/5387 BC and younger via radiocarbon and AMS dating in the nearby trench (Falcucci *et al.* 2009; Galli *et al.* 2009; Boncio *et al.* 2010). Here, several convex-upwards radar returns may be evidence of channels-like features, but we are wary of this interpretation as flow in the channels would be oblique to the slope. Like Site 1, there is some uncertainty as to the exact position of the base Holocene in the hangingwall of the fault, but the vertical offset of the base Holocene is in the range of 2.0–3.5 m, with uncertainty produced by the possible air-return hyperbolae. This suggests a post-base-Holocene throw-rate of 0.23–0.13 mm yr^{-1} assuming an age for this contact of 15 ka. This rate should be compared to that implied from the offset of the top of the cemented white conglomerate (3.5 m offset; 33 ka; 0.11 mm yr^{-1}), assuming its age is 33 ka. Again, the white, cemented conglomerate, and an underlying unit that is not exposed at outcrop with less clear radar returns, may show 'lap' relationships with underlying angular unconformities near the base of imaged section. Again, we tentatively interpret these as offlap of alluvial fan sediments above basal erosional truncation surfaces. The base of the section is not well imaged so again, we are uncertain of the offset of these older units at depth. We note that there is one clear example where the radar had poor contact with the ground, producing a delay, and hence vertical feature that continues to the surface. However, we have interpreted two other vertical features as faults rather than artefacts of poor radar contact, because these vertical discontinuities do not continue to the surface, with continuous layers across them at the shallowest levels. Note that Site 2, with clear Holocene offset, was not ruptured in 2009, as the rupture occurs at a higher elevation on the fault escarpment, at Site 3. Thus, despite the problem with possible air returns, our working hypothesis is that this site has a throw-rate of 0.23–0.13 mm yr^{-1} assuming an age for this contact of 15 ka; confirmation of this working hypothesis requires additional data from shallow geophysics, or a trench excavation.

Site 3 shows a similar radar return stratigraphy to Site 2. Thin, continuous and parallel radar returns are truncated at depth by a fault, so again we interpret this as downfaulting of the white, cemented (>25–33 ka) conglomerates that crop out in the nearby trench. Again, an angular unconformity separates this unit from overlying deposits that we interpret to be the ceramic-bearing, organic-rich colluvial conglomerates, sandstones and soil that have been dated to 5718 BC/5467 BC to 5403 BC/5387 BC or younger. The up-dip continuation of the fault through the Holocene deposits is unclear on the GPR data, but field observations show that this site was ruptured in 2009, because a set of cracks with 5–7 cm vertical downthrow to the SW was observed on a hairpin bend in a tarmac road. The vertical offset of the base of the Holocene appears to be no greater than 1.5 m, implying a throw-rate of 0.1 mm yr^{-1} assuming an age for this contact of 15 ka. This rate is similar to that implied from the offset of the top of the cemented white conglomerate (3 m offset; 33 ka; 0.09 mm yr^{-1}), assuming its age is 33 ka. Again, the base of the section is not well imaged so we are unsure of the offsets and hence implied throw-rates for these older units.

5.3 Site 4–concrete road 420 m SE of the water pipe

Site 4 is a 70-m long survey running NE–SW across the rupture that achieved depth penetration of about 7–10 m on a topographic slope that decreased in elevation by 36 m over a horizontal distance of 70 m (Fig. 8). The rupture exhibited about 7 cm of vertical offset at this site. A study of post-seismic deformation using LiDAR demonstrates afterslip at this site and growth in amplitude and wavelength of a post-seismic hangingwall syncline (Wilkinson *et al.* 2010). Although conglomerates are exposed 60 m to the NNW in a small quarry, there are no outcrops nearby that are along strike from the GPR survey. Thus, any interpretations of the subsurface stratigraphy are more subjective than those for Sites 1, 2 and 3; the radar returns are also less clear, with less spatially complete depth penetration than for Sites 1, 2 and 3. Also, as for Site 2, we have some concerns about possible air returns, in this case from a concrete post carrying electricity power cables (Fig. 8). However, despite a possible example of a long wavelength hyperbola, consistent with an air return from the post and power cables, we think sufficient subsurface geology has been imaged by the GPR to make an interpretation of the Holocene throw-rate. However, we feel the interpretation of this site may be less robust than that for Sites 1, 2 and 3.

The GPR data show layered stratigraphy, and appear to reveal a faulted offset of the base of this layered sequence at a depth of 4–5 m below the 7 cm offset surface rupture on the concrete road. A second fault offsets the base of the layered unit, about 10 m into the footwall of the rupture, again coincident with a surface crack (1 cm opening with 4 mm throw) observed on the concrete road. The surface that we interpret to be offset is an angular unconformity at the base of the layered stratigraphy (Fig. 8b). We tentatively interpret vertical offsets of 70 cm across each of the two aforementioned faults, although we note this is close to the resolution of the data. Beneath this angular unconformity, we interpret a syncline defined by relatively weak radar returns that cross the long wavelength hyperbola that may be due to the electricity pole. Thus, these relatively weak radar returns are likely to be real geological layers rather than air returns. This syncline is in the same location as the post-seismic hangingwall syncline that has been shown to have grown using repeated LiDAR surveys (Wilkinson *et al.* 2010). The LiDAR data are thus consistent with our interpretation of a hangingwall syncline imaged with GPR. Two localized, vertically stacked sets of radar returns within the syncline may mark discontinuities associated with fractures. The interpreted syncline, and the layered stratigraphy have not been dated. However, if we assume that the hangingwall-layered radar stratigraphy correlates with the ceramic-bearing, organic-rich colluvial conglomerates, sandstones and soil that have been dated to 5718 BC/5467 BC to 5403 BC/5387 BC or younger (Falcucci *et al.* 2009; see also Galli *et al.* 2009; (Boncio *et al.* 2010), the implied throw rate is 0.08–0.09 mm yr^{-1}, assuming an age for the base of the layered stratigraphy of 18–15 ka. However, if the stratigraphy within the syncline is also Holocene, the implied throw rate is 0.25–0.3 mm yr^{-1}, again assuming an age for the base of the syncline sequence of 18–15 ka; we prefer this latter interpretation (A plus C in Fig. 8b), but only because it reveals a similar throw-rate to that from Site 1; clearly this needs more work, perhaps in the form of a palaeoseismic trench study.

5.4 Summary

The ground-penetrating radar data from the four sites and rupture observations define two major subparallel, but en-echelon faults within the Paganica fault zone (Fig. 3). All four sites display Holocene throws, and three show late Pleistocene throws. Throws vary along strike defining throw-gradients (Fig. 9). The throw and throw-rate gradients, and the map geometry of the faults define a relay zone (Figs 3a and e, Fig. 9). Existence of the relay zone may explain possible examples of channels in the Holocene deposits whose flow was oblique to the overall slope, perhaps influenced by oblique ground warping of the relay ramp. The 2009 rupture stepped across this relay zone, but the slip-vector azimuth was constant across this structure (Fig. 4). Rates of throw accumulation implied by vertical offset of Holocene and older layers are consistent through time. When summed across strike, the combined throw-rate across these two faults, averaged since 15 ka, is a maximum of 0.23–0.30 mm yr^{-1} (Fig. 3e), although higher values may exist if (a) throw-gradients continue away from the area studied, or (b) other faults active in the Holocene, but unknown to us, lie across strike. Another relay zone, not imaged by GPR, but clear on the published rupture maps exist ∼200 m WNW of the ruptured water pipe. Other examples of relay zones are clear in the rupture map provided by ISPRA Report (2009); Boncio *et al.* (in press) and Emergeo Working Group (2009) located ∼1 km to the ESE of the ruptured water pipe.

6 DISCUSSION

The surface ruptures to the 2009 earthquake occurred within the Paganica fault zone. However in detail they occurred along a subtle escarpment in the hangingwall of the main fault shown on the geological map of Vezzani & Ghisetti (1998) (Fig. 1d). This hangingwall fault is itself subdivided into at least two active fault strands that both show Holocene displacements revealed by ground-penetrating radar (Fig. 3), and several others revealed by observations of at least four faults in Pleistocene gravels exposed in the trench excavated by water escape along the ruptured water pipe. The rate of throw accumulation (0.23–0.30 mm yr^{-1}; Fig. 3e) is relatively low compared to other faults around L'Aquila (see Table 1, and Vezzani & Ghisetti 1998; Galadini & Galli 2000; Galli *et al.* 2002; Pizzi *et al.* 2002; Roberts & Michetti 2004; Papanikolaou *et al.* 2005; Galli *et al.* 2008), suggesting this is an example of a Type 3 scarp, as defined earlier. The throw-rate of 0.23–0.30 mm yr^{-1} suggests that the Paganica fault zone cannot accommodate all of the 3–5 mm yr^{-1} extension known for this sector of the Apennines (D'Agostino *et al.* 2008; see also Roberts & Michetti 2004); other faults have a role to play. Although our observations do not rule out the possibility that the 1461 AD and 1762 AD earthquakes

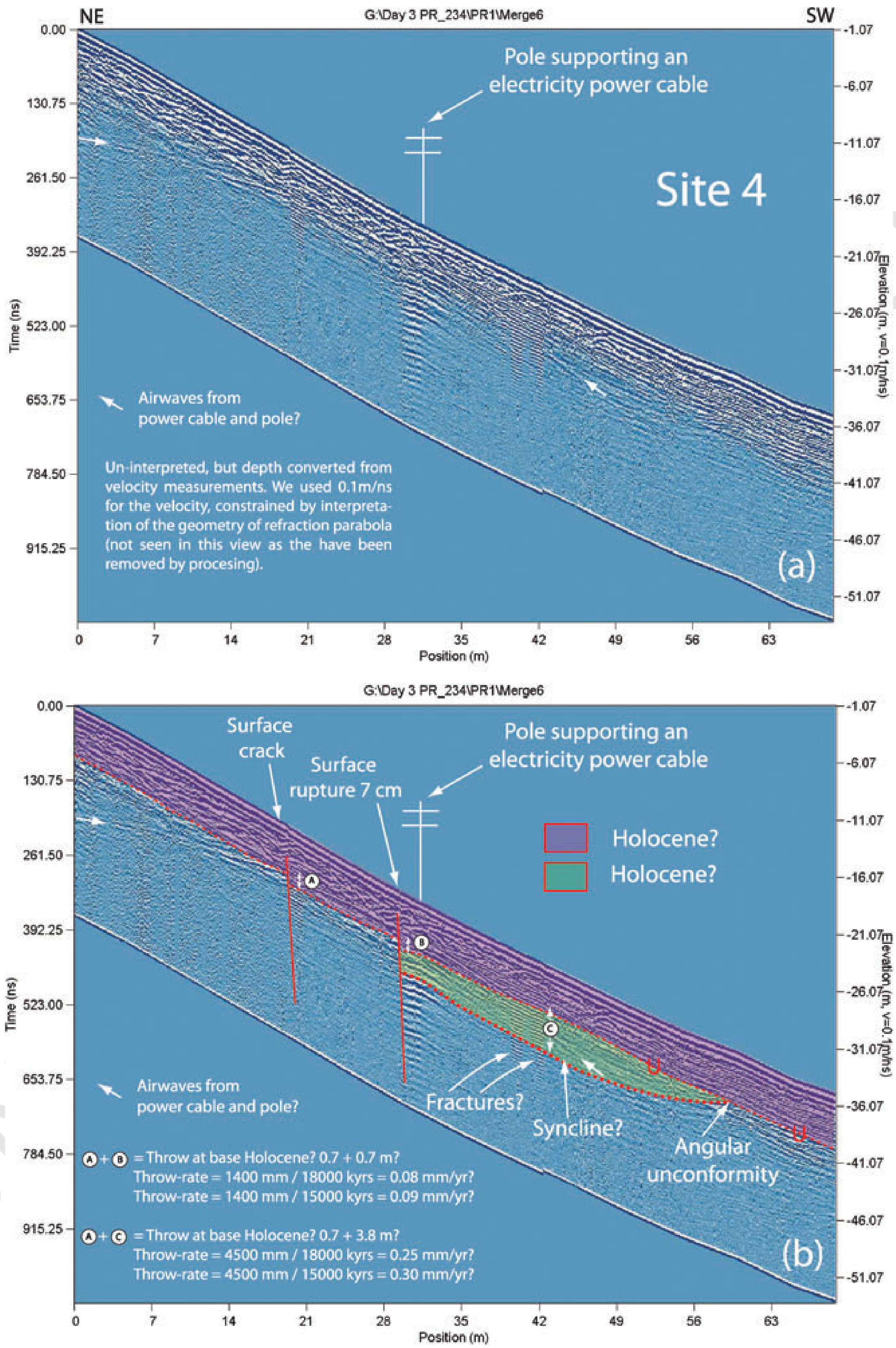

Figure 8. Site 4 (a) Un-interpreted, and (b) interpreted depth converted ground-penetrating radar profiles. Vertical scales are time in nanoseconds and depth in metres. The profile was collected on a concrete road. Convex upwards hyperbolae in the upper part of the section are interpreted to be from point sources (subsurface boulders?). The long wavelength hyperbolae centred on the 7 cm surface rupture may be an air return from a pole supporting an electricity power cable. Q15

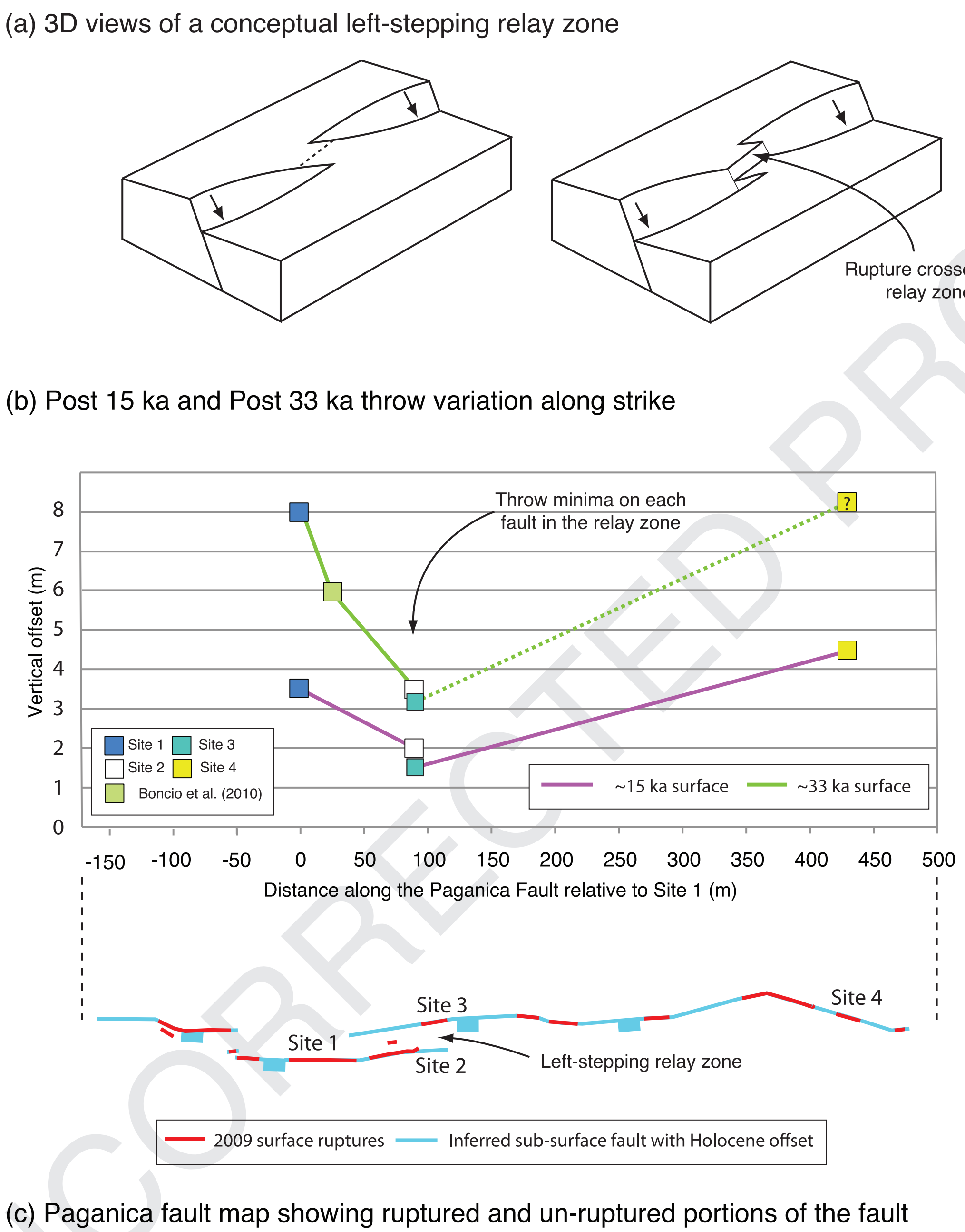

Figure 9. Throw-gradients along strike for ∼15 ka and ∼33 ka surfaces.

occurred within the Paganica fault zone, the relatively low throw-rate we have measured suggests this may be unlikely, because as pointed at by Tertulliani *et al.* (2009), the implied recurrence interval seems very short. In Fig. 1 we suggest alternative locations for the surface ruptures to the 1461 AD and 1762 AD earthquakes based on the locations of towns damaged at Mercalli intensity >IX documented in the website http://storing.ingv.it/cfti4med/. Although we have not proved these rupture locations are correct in this paper, or better than those suggested by Tertulliani *et al.* (2009), they provide an alternative to recurrence of $>M6$ earthquake on the Paganica fault with '∼three centuries recurrence intervals'. The locations we suggest occur along well-known faults with relatively high slip-rates (Table 1, e.g. Vezzani & Ghisetti 1998; Galadini & Galli 2000; Galli *et al.* 2002; Roberts & Michetti 2004; Papanikolaou *et al.* 2005; Galli *et al.* 2008). Given the uncertainty in historical shaking intensity reports described by Tertulliani *et al.* (2009), we doubt the surface rupture locations we suggest can be differentiated from repeated rupture of the Paganica fault based on these data alone, because shaking intensity is probably more sensitive to site conditions and building vulnerability than differences in epicentral distance of a few kilometres. Clearly, palaeoseismological studies are needed to differentiate between possible sites for the ruptures to the 1461 and 1762 AD earthquakes.

With hindsight, it is now clear that the incised drainage in the footwall of the Paganica fault was perhaps the only obvious indicator of fault activity prior to the earthquake, due to the relatively low throw-rate on this fault in the Holocene (Type 3 scarp). It is clear that such incised drainage patterns should be utilized in the ongoing search for active normal faults in the Italian Apennines and elsewhere (e.g. Roberts 2008). However, it must be borne in mind that other indicators of fault activity, such as bedrock scarps (Type 1) and faulted alluvial fans seen in palaeoseismic trenches (Type 2) should not be forgotten. Although tragic, we must not focus our attention with regard to seismic hazard in central Italy solely on the Paganica Fault; neighbouring range-bounding normal faults, marked by bedrock scarps and faulted alluvial fans and moraines, have higher throw-rates (Table 1), and are known to slip in metre-sized events in destructive earthquakes evidenced by dating of colluvial wedges in trenches (Galli *et al.* 2008), cosmogenic exposure dating (Palumbo *et al.* 2004) and historical observations (Oddone 1915); the probability of rupture of one of these faults in a given time period, assuming similar-sized slip events, will be higher than that for the Paganica fault if they have higher throw-rates.

7 CONCLUSIONS

Observations with ground-penetrating radar reveal how the surface rupture to the April 6 L'Aquila earthquake relates spatially to previous surface displacements during the Holocene and Pleistocene. In Paganica, the discontinuous surface rupture stepped across a relay zone between en-echelon/parallel faults. Some portions of the fault zone that show clear Holocene offsets were not ruptured in 2009, having been bypassed as the rupture stepped across a relay zone onto a fault across strike. The slip-vector azimuth, defined by opening directions across surface cracks, shows dip-slip motion, and remained constant between 210–228° across the zone where the rupture stepped between faults. Maximum vertical offsets of the base of the Holocene summed across strike are 4.5 m, which if averaged over 15 kyrs, gives a throw-rate of 0.23–0.30 mm yr^{-1}. The values are consistent with throw-rate values implied by offsets of an older layer whose age we assume is ~33ka. The post-base-Holocene and post-~33 ka throw-rate values compare with published values of 0.4 mm yr^{-1} for a minimum throw-rate implied by the vertical offset of Middle Pleistocene tephras (Messina *et al.* 2009), and a throw-rate 0.24 mm yr^{-1} since 24.8 kyr from a palaeoseismic trench study (Boncio *et al.* 2010). The Paganica fault, although clearly an important active structure, is not slipping fast enough to accommodate all of the 3–5 mm yr^{-1} of extension across this sector of the Apennines. Other neighbouring range-bounding active normal faults also have an important role to play in the seismic hazard. These faults have slip-rates that are generally higher than that displayed by the Paganica fault, suggesting that, on average, they will have shorter earthquake recurrence intervals for a given earthquake magnitude.

ACKNOWLEDGMENTS

This study was funded by NERC Urgency Grant NE/H003266/1, and NERC Standard Grant NE/E01545X/1, with support from WP4.5 from the INGV. We acknowledge the work of Cinti *et al.* (in preparation) in enlarging the trench cut by the ruptured water pipe; the newly exposed sediments improved our interpretation.

REFERENCES

Anderson, H. & Jackson, J., 1987. Active tectonics of the Adriatic region, *Geophys. J. R. astr. Soc.,* **91,** 937–983.

APAT, 2005. Carta Geologica d'Italia alla scala 1:50,000, Sheet 359, L'Aquila, S.EL.CA., Firenze, 2006.

Atzori, S. *et al*., 2009. Finite fault inversion of DInSAR coseismic displacement of the 2099 L'Aquila earthquake (central Italy), *Geophys. Res. Lett.,* **36,** L15305, doi:10.1029/2009GL039293.

Bagnaia, R., D'Epifanio, A. & Sylos Labini, S., 1992. Aquila and subaequan basins: an example of Quaternary evolution in central Apennines, Italy, Quat. Nova, II, 187–209. Q16

Barchi, M. *et al*.,(eds) 2000. Sintesi *Delle Conoscenze Sulle Faglie Attive in Italia Centrale: Parametrizzazione Ai fini Della Carattrizzazione Della Pericolosita' Sismica,* CNR-GNDT, Rome, 62 pp. Q17

Basili, R., Valensise, G., Vannoli, P., Burrato, P., Fracassi, U., Mariano, S., Tiberti, M.M. & Boschi, E., 2008.The database of individual seismogenic sources (DISS), version 3: summarizing 20 years of research on Italy's earthquake geology, *Tectonophysics,* **453**(1–4), 20–43.

Bertini T. & Bosi C., 1993. Lat tettonica quaternaria della conca di Fossa (L'Aquila). *Il Quaternario,* **6,** 293–314.

Blumetti, A. M., 1995. Neotectonic investigations and evidence of paleoseismicity in the epicentral area of the January-February 1703, Central Italy, earthquakes, *Bull. assoc. Eng. Geol., Special Publication No. 6 "Perspectives in Paleoseismology",* 83–100.

Blumetti, A.M., Dramis, F. & Michetti, A.M., 1993. Fault-generated mountain fronts in the central Apennines (central Italy): geomorphological features and seismotectonic implications. *Earth Surf. Process. Landf.,* **18,** 203–223.

Boncio, P., Lavecchia, G. & Pace, B., 2004. Defining a model of 3D seismogenic sources for seismic hazard assessment applications: the case of central Apennines (Italy), *J. Seismol.,* **8,** 407–425, doi:10.1023/B:JOSE.0000038449.78801.05.

Boncio, P., Pizzi, A., Brozzetti, G., Pomposo, G., Lavecchia, G., Di Naccio, D. & Ferrarini, F., 2010. Coseismic ground deformation of the 6 April 2009 L'Aquila earthquake (central Italy, Mw6.3), *Geophys. Res. Lett.,* **37,** L06308, doi:10.1029/2010GL042807, 2010. Q18

Bosi, C., 1975. Osservazioni preliminari su faglie probabilmente attive nell'Appennino centrale, *Boll. Soc. Geol. It.,* **94,** 827–859.

1962. Carta Geologica d'Italia 1:100000, 140, Teramo. Servizio Geologico d'Italia. Q19

Chiarabba, C. *et al*., 2009. The 2009 L'Aquila (central Italy) Mw6.3 earthquake: main shock and aftershocks, *Geophys. Res. Lett.,* **36,** L18308, doi:10.1029/2009GL039627.

D'Addezio, G., Pantosti, D. & de Martini, P. M., 1996. Palaeoseismologic and geomorphic investigations along the middle portion of the Ovindoli-Pezza Fault (Central Italy), *Annali di Geofisica,* **XXXIX**, 663–675.

D'Addezio G., Masana E. & Pantosti D., 2001. The Holocene paleoseismicity of the Aremogna-Cinque Miglia Fault (Central Italy), *J. Seismol.,* **5,** 181–205.

D'Agostino, N., Avallone, A., Cheloni, D., D'Anastasio, E., Mantenuto, S. & Selvaggi, G., 2008. Active tectonics of the Adriatic region from GPS and earthquake slip vectors, *J. geophys. Res.,* **113,** B12413, doi:10.1029/2008JB005860.

Emergeo Working Group, 2009. Evidence for surface rupture associated with the Mw 6.3 L'Aquila earthquake sequence of April 2009, central Italy, *Terra Nova,* 43–51, doi:10.1111/j.1365-3121.2009.00915.x.

Falcucci, E. *et al*., 2009. The Paganica Fault and surface coseismic ruptures caused by the 6 April 2009 Earthquake (L'Aquila, central Italy), *Seismol. Res. Lett.,* **80**(6), 940–950.

Faure, W.J., Roberts, G.P., Cowie, P.A., Papanikolaou, I., Michetti, A.M., Sammonds, P. & Phillips, R., 2009. Horizontal strain-rates and throw-rates across breached relay-zones, central Italy: implications for the preservation of throw deficits at points of normal fault linkage, *J. Struct. Geol.,* **31,** 1145–1160, doi:10.1016/j.jsg.2009.06.01.

Faure Walker, J., 2010. Mechanics of continental extension from Quaternary strain fields in the Italian Apennines, *Unpublished PhD thesis*. University College London.

Galadini, F. & Galli, P., 2000. Active tectonics in the central Apennines (Italy): input data for seismic hazard assessment, *Nat. Hazards,* **22,** 225–270.

Galli, P., Galadini, F., Moro, M. & Giraudi, C., 2002. New paleoseismological data from the Gran Sasso d'Italia area (central Apennines), *Geophys. Res. Lett.,* **29**(7), doi:10.1029/2001GL013292.

Galli, P., Galadini, F. & Pantosti, D., 2008. Twenty years of palaeoseismology in Italy, *Earth-Sci. Rev.,* **88,** 80–117.

Galli, P. *et al*., 2009. Il terremotto Aquilano del 6 Aprile 2009: rilievo macrosismico, effetti di superficie ed implicazioni sismotettoniche, *Il Quaternario,* **22**(2), 235–246.

Giraudi, C. & Frezzotti, M., 1995. Paleoseismicity in the Gran Sasso Massif (Abruzzo, Central Italy), *Quaternary International,* **25,** 81–93.

ISPRA Report, 2009. Geological effects induced by the L'Aquila earthquake (6 April 2009, MI = 5.8) on the natural environment: preliminary report, Available at http://www.apat.gov.it/site/en-GB/Projects/INQUA_Scale/Documents/

Q20

Jewell, C. & Bristow, C., 2004. GPR studies in the Piano di Pezza area o the Ovindoli-Pezza Fault, Central Apennines, Italy: extending palaeoseismic trench investigations with high resolution GPR profiling, in *Proceedings of Tenth International Conference on Ground Penetrating Radar,* 21–24 June, Delft, The Netherlands. 555–558.

Messina, A.P., Galli, P., Giaccio, B. & Peronace, E., 2009. Quaternary tectonic evolution of the area affected by the Paganica fault (2009 L'Aquila earthquake), in *Proceedings of 28° GNGTS National Conference, Trieste 16–19 November 2009, Abstracts Volume,* 47–50.

Michetti, A.M., Serva, L. & Vittori, E., 2000. ITHACA Italy hazard from capable faults: a database of active faults of the Italian onshore territory. CD-Rom and explicative notes, ANPA (copies available from E. Vittori: vittori@anpa.it).

Oddone, E., 1915. Gli elementi fisica del grande terremoto marsicano fucense del 13 Gennaio 1915, *Boll. Soc. sismol. Ital.,* **19,** 71–215.

Pace, B., Boncio, P. & Lavecchia, G., 2002. The 1984 Abruzzo earthquake (Italy): an example of seismogenic process controlled by interaction between differently oriented synkinematic faults, *Tectonophysics,* **350,** 237–254.

Pace, B., Peruzza, L., Lavecchia, G. & Boncio, P., 2006. Layered seismogenic source model and probabilistic seismic hazard analyses in central Italy, *Bull. seism. Soc. Am.,* **96**(1), 107–132.

Palumbo, L., Benedetti, L., Bourles, D., Cinque, A. & Finkel, R., 2004. Slip history of the Magnola fault (Apennines, Central Italy) from ^{36}Cl surface exposure dating: evidence for strong earthquakes over the Holocene, *Earth planet. Sci. Lett.,* **225,** 163–176.

Pantosti, D., D'Addezio, G. & Cinti, F., 1996. Paleoseismicity of the Ovindoli-Pezza fault, central Apennines, Italy: a history including a large, previously unrecorded earthquake in the Middle Ages (860–1300 A.D.), *J. geophys. Res.,* **101,** 5937–5960.

Papanikolaou, I, Roberts, G.P. & Michetti, A.M., 2005. Fault scarps and deformation rates in Lazio-Abruzzo, Central Italy: comparison between geological fault slip-rate and GPS data, *Tectonophysics,* **408,** 147–176.

Papanikolaou, I.D., Foumelis, M., Parcharidis, I., Lekkas, E.L. & Fountoulis, I.G., 2010. Deformation pattern of the 6th and 7 April 2009, Mw = 6.3 and Mw = 5.6 earthquakes in L'Aquila (Central Italy) revealed by ground and space based observations, *Nat. Hazards Earth Syst. Sci.,* **10,** 73–87.

Piccardi, L., Gaudemer, Y., Tapponier, P. & Boccaletti, M., 1999. Active oblique extension in the central Apennines (Italy): evidence from the Fucino region, *J. geophys. Int.,* **139,** 499–530.

Pizzi, A., Calmita, F., Coltorti, M. & Pieruccini, P., 2002. Quaternary normal faults, intramontane basins and seismicity in the Umbria-Marche Apennines Ridge (Italy): contribution of neotectonic analysis to seismic hazard assessment, *Boll. Soc. Geol. It.,* Volume speciale n. **1,** 923–929.

Roberts, G. P., 2008. Visualisation of active normal fault scarps in the Apennines, Italy: a key to assessment of tectonic strain release and earthquake rupture, in *Google Earth Science, Journal of the Virtual Explorer,* Vol. **30**, ed. De Paor, D., Electronic Edition, ISSN 1441–8142, pp. 3.

Roberts, G.P. & Michetti, A.M., 2004. Spatial and temporal variations in growth rates along active normal fault systems: an example from Lazio-Abruzzo, central Italy, *J. Struct. Geol.,* **26,** 339–376.

Roberts, G.P., Cowie, P., Papanikolaou, I. & Michetti, A.M., 2004. Fault scaling relationships, deformation rates and seismic hazards: an example from Lazio-Abruzzo region, central Italy, *J. Struct. Geol.,* **26,** 377–398.

Salvi, S., Cinti, F.R., Colini, L., D'Addezio, G., Doumaz, F. & Pettinelli, E., 2003. Investigations of the active Celano-L'Aquila fault system, Abruzzi (central Apennines, Italy) with combined ground-penetrating radar and palaeoseismic trenching, *Geophys. J. Int.,* **155,** 805–818.

Schlagenhauf, A., 2010. Identification des forts seismes passes sur les failles normales actives de la region Lazio-Abruzzo (Italie centrale) par "datations cosmogeniques" (^{36}Cl) de leurs escarpments, *These, Docteur* de l'Universite Joseph Fourier, Grenoble, France.

Q21

Tertulliani, A., Rossi, A., Cucci, L. & Vecchi, M., 2009. L'Aquila (Central Italy) earthquakes: the predecessors of the April 6, 2009 event, *Seismol. Res. Lett.,* **80**(6), 1008.

Q22

Uria de Llanos, A., 1703, Relazione overo itinerario fatto dall'auditore Alfonso Uria del Llanos per riconoscere li danni causati dalli passati terremoi seguiti li 14 Gennaro e 2 Febraro M.DCCIII: stamperi Gaetano Zenobj, Roma.

Valensise, G. & Pantosti,D., 2001a. The investigation of potential earthquake sources peninsular Italy: a review, *J. Seismol.,* **5**(3), 287–306.

Valensise, G. & Pantosti, D., (Editors). 2001b. Database of potential sources for earthquakes larger than M5.5 in Italy, *Ann. Geofis.,* **44**(suppl.), 180, with CD-ROM.

Vezzani, L. & Ghisetti, F., 1998. Carta Geologica Dell'Abruzzo, 1:100000, SELCA, Via R. Giuliani, 153—Firenze.

Vittori, E., 1994. Project of a map and database of active faults in Italy: methodological approach, in *Proceedings of Scientific Meeting on the Seismic Protection,* pp. 119–130, ed. Spagna, V., Giunta Regionale del Veneto, Palazzo Balbi, Venice, July 12–13 1993.

Walters, R.J. *et al*., 2009. The 2009 L' Aquila Earthquake (Central Italy): a source mechanism and implications for seismic hazard, *Geophys. Res. Lett.,* **36,** L17312, doi:10.1029/2009GL039337.

Wells, D.L. & Coppersmith, K.J., 1994. New empirical relationships among magnitude, rupture length, rupture width, rupture area, and surface displacement, *Bull. seism. Soc. Am.,* **84**(4), 974–1002.

Wilkinson, M. *et al*., 2010. Partitioned postseismic deformation associated with the 2009 Mw 6.3 L'Aquila earthquake surface rupture measured using a terrestrial laser scanner, *Geophys. Res. Lett.,* **37,** L10309, doi:10.1029/2010GL043099.

Queries

Journal: GJI
Paper: gji_4713

Dear Author

During the copy-editing of your paper, the following queries arose. Please respond to these by marking up your proofs with the necessary changes/additions. Please write your answers on the query sheet if there is insufficient space on the page proofs. Please write clearly and follow the conventions shown on the corrections sheet. If returning the proof by fax do not write too close to the paper's edge. Please remember that illegible mark-ups may delay publication.

Query Reference	Query	Remarks
Q1	Author: please check and confirm that you are happy with the section (shown on the right-hand side of the title page) to which this paper has been assigned: a list of all the sections can be found in the Author Guidelines (http://www.wiley.com/bw/submit.asp?ref=0956-540X&site=1).	
Q2	Author: Please provide a maximum of up to six keywords from the list attached.	
Q3	Author: Spelling of author name Papanikolaou in the reference Papanikolaou *et al.* (2010) has been changed to match the spelling in the Reference List. Please confirm that this is correct.	
Q4	Author: Spelling of author name Basili in the reference Basili *et al.* (2008) has been changed to match the spelling in the Reference List. Please confirm that this is correct.	
Q5	Author: Reference Vezzani & Ghisetti (1987) has not been included in the Reference List, please supply full publication details.	
Q6	Author: A running head short title was not supplied; please check if this one is suitable and, if not, please supply a short title of up to 45 characters that can be used instead.	
Q7	Author: Westaway & Jackson 1987 has not been included in the Reference List, please supply full publication details.	
Q8	Author: Pantosti *et al.* 1993 has not been included in the Reference List, please supply full publication details.	
Q9	Author: Please check the term Quaternary? appearing in the table body for correctness.	
Q10	Author: Michetti *et al.* 1996 has not been included in the reference list; please supply full publication details.	

Q11	Author: Please check the term '(Miocene?)' in the sentence 'The hangingwall Holocene-Pleistocene sediments are suggested . . . at 30–70 m depth' for correctness.	
Q12	Author: Please proide the expanded form of 'GPR'.	
Q13	Author: Please provide the expanded form of 'AMS'.	
Q14	Author: Please update the reference Boncio *et al.* (in press) if it has been published also please provide the complete publishing details of the same in the reference list.	
Q15	Author: Please check the term 'subsurface boulders?' appearing in figure legends 6 and 8 for correctness.	
Q16	Author: Please provide the volume number for the reference Bagnaia *et al.* (1992).	
Q17	Author: Please check reference Barchi et al. (2000) for correctness.	
Q18	Author: The publication year of Boncio et al. (2010) has been inserted to match the publication year given in the text. Please confirm that this is correct.	
Q19	Author: Please check the reference Carta Geologica d'Italia (1962) for correctness.	
Q20	Author: Please provide the last accessed date of the URL in the reference ISPRA Report (2009).	
Q21	Author: The publication year of Schlagenhauf (2010) has been inserted to match the publication year given in the text. Please confirm that this is correct.	
Q22	Author: The publication year of Tertulliani et al. (2009) has been inserted to match the publication year given in the text. Please confirm that this is correct. Also, Please supply the doi code or page range (or both) for the same, or indicate if it is a one-page reference.	

Key words

Authors are requested to choose key words from the list below to describe their work. The key words will be printed underneath the summary and are useful for readers and researchers. Key words should be separated by a semi-colon and listed in the order that they appear in this list. An article should contain no more than six key words.

GEOPHYSICAL METHODS
Time series analysis
Image processing
Neural networks, fuzzy logic
Numerical solutions
Fourier analysis
Wavelet transform
Instability analysis
Inverse theory
Numerical approximations and analysis
Persistence, memory, correlations, clustering
Probabilistic forecasting
Spatial analysis
Downhole methods
Tomography
Interferometry
Thermobarometry
Fractals and multifractals
Non-linear differential equations
Probability distributions
Self-organization

GEODESY and GRAVITY
Satellite geodesy
Reference systems
Sea level change
Space geodetic surveys
Seismic cycle
Transient deformation
Gravity anomalies and Earth structure
Geopotential theory
Time variable gravity
Earth rotation variations
Global change from geodesy
Lunar and planetary geodesy and gravity
Radar interferometry
Plate motions
Tides and planetary waves
Acoustic-gravity waves

GEOMAGNETISM and ELECTROMAGNETISM
Electrical properties
Electromagnetic theory
Magnetotelluric
Non-linear electromagnetics
Archaeomagnetism
Biogenic magnetic minerals
Dynamo: theories and simulations
Environmental magnetism
Geomagnetic excursions
Geomagnetic induction
Ground penetrating radar
Magnetic anomalies: modelling and interpretation
Magnetic and electrical properties
Magnetic fabrics and anisotropy
Magnetic mineralogy and petrology
Magnetostratigraphy
Palaeointensity
Palaeomagnetic secular variation
Palaeomagnetism applied to tectonics
Palaeomagnetism applied to geologic processes
Rapid time variations
Remagnetization
Reversals: process, time scale, magnetostratigraphy
Rock and mineral magnetism
Satellite magnetics
Marine magnetics and palaeomagnetics
Marine electromagnetics

GENERAL SUBJECTS
Geomorphology
Geomechanics
Glaciology
Hydrogeophysics
Ionosphere/atmosphere interactions
Ionosphere/magnetosphere interactions
Gas and hydrate systems
Ocean drilling
Hydrology
Ultra-high pressure metamorphism
Ultra-high temperature metamorphism
Tsunamis
Thermochronology
Heat flow
Hydrothermal systems
Mantle processes
Core, outer core and inner core

COMPOSITION and PHYSICAL PROPERTIES
Microstructures
Permeability and porosity
Plasticity, diffusion, and creep
Composition of the core
Composition of the continental crust
Composition of the oceanic crust
Composition of the mantle
Composition of the planets
Creep and deformation
Defects
Elasticity and anelasticity
Equations of state
High-pressure behaviour
Fracture and flow
Friction
Fault zone rheology
Phase transitions

SEISMOLOGY
Controlled source seismology
Earthquake dynamics
Earthquake ground motions
Earthquake source observations
Seismic monitoring and test-ban treaty verification
Palaeoseismology
Earthquake interaction, forecasting, and prediction
Seismicity and tectonics
Body waves
Surface waves and free oscillations
Interface waves
Guided waves
Coda waves
Seismic anisotropy
Seismic attenuation
Site effects
Seismic tomography
Volcano seismology
Computational seismology
Theoretical seismology
Statistical seismology
Wave scattering and diffraction
Wave propagation
Acoustic properties
Early warning
Rheology and friction of fault zones

TECTONOPHYSICS
Planetary tectonics
Mid-ocean ridge processes
Transform faults
Subduction zone processes
Intra-plate processes
Volcanic arc processes
Back-arc basin processes
Cratons
Continental margins: convergent
Continental margins: divergent
Continental margins: transform
Continental neotectonics
Continental tectonics: compressional
Continental tectonics: extensional
Continental tectonics: strike-slip and transform
Sedimentary basin processes
Oceanic hotspots and intraplate volcanism
Oceanic plateaus and microcontinents
Oceanic transform and fracture zone processes
Submarine landslides
Submarine tectonics and volcanism
Tectonics and landscape evolution
Tectonics and climatic interactions
Dynamics and mechanics of faulting
Dynamics of lithosphere and mantle
Dynamics: convection currents, and mantle plumes
Dynamics: gravity and tectonics
Dynamics: seismotectonics
Heat generation and transport

Impact phenomena
Hotspots
Large igneous provinces
Lithospheric flexure
Obduction tectonics
Neotectonics
Diapir and diapirism
Folds and folding
Fractures and faults
Kinematics of crustal and mantle deformation
High strain deformation zones
Crustal structure
Mechanics, theory, and modelling
Rheology: crust and lithosphere
Rheology: mantle

PLANETS
Planetary interiors
Planetary volcanism

VOLCANOLOGY
Physics of magma and magma bodies
Magma chamber processes
Magma genesis and partial melting
Pluton emplacement
Effusive volcanism
Mud volcanism
Subaqueous volcanism
Explosive volcanism
Volcaniclastic deposits
Volcano/climate interactions
Atmospheric effects (volcano)
Volcanic gases
Lava rheology and morphology
Magma migration and fragmentation
Eruption mechanisms and flow emplacement
Physics and chemistry of magma bodies
Calderas
Experimental volcanism
Tephrochronology
Remote sensing of volcanoes
Volcano monitoring
Volcanic hazards and risks

GEOGRAPHIC LOCATION
Africa
Antarctica
Arctic region
Asia
Atlantic Ocean
Australia
Europe
Indian Ocean
New Zealand
North America
Pacific Ocean
South America

MARKED PROOF

Please correct and return this set

Please use the proof correction marks shown below for all alterations and corrections. If you wish to return your proof by fax you should ensure that all amendments are written clearly in dark ink and are made well within the page margins.

Instruction to printer	*Textual mark*	*Marginal mark*
Leave unchanged	• • • under matter to remain	
Insert in text the matter indicated in the margin		New matter followed by or
Delete	/ through single character, rule or underline or through all characters to be deleted	or
Substitute character or substitute part of one or more word(s)	/ through letter or through characters	new character / or new characters /
Change to italics	— under matter to be changed	
Change to capitals	under matter to be changed	
Change to small capitals	under matter to be changed	
Change to bold type	under matter to be changed	
Change to bold italic	under matter to be changed	
Change to lower case	Encircle matter to be changed	
Change italic to upright type	(As above)	
Change bold to non-bold type	(As above)	
Insert 'superior' character	/ through character or where required	or under character e.g. or
Insert 'inferior' character	(As above)	over character e.g.
Insert full stop	(As above)	
Insert comma	(As above)	,
Insert single quotation marks	(As above)	or and/or or
Insert double quotation marks	(As above)	or and/or or
Insert hyphen	(As above)	
Start new paragraph		
No new paragraph		
Transpose		
Close up	linking characters	
Insert or substitute space between characters or words	/ through character or where required	
Reduce space between characters or words	| between characters or words affected	